

**INFLUENCE OF SPECTRAL BEAM SPLITTING ON THE  
PERFORMANCE OF POLYCRYSTALLINE SILICON PV CELLS**

CO Agutu

12055532

Department of Chemical Engineering

University of Pretoria

# **INFLUENCE OF SPECTRAL BEAM SPLITTING ON THE PERFORMANCE OF POLYCRYSTALLINE SILICON PV CELLS**

Dissertation submitted in partial fulfilment of the  
requirements for the Masters in Engineering

CO Agutu

12055532

07/02/2018

# INFLUENCE OF SPECTRAL BEAM SPLITTING ON THE PERFORMANCE OF POLYCRYSTALLINE SILICON PV CELLS

## Abstract

This report determines the influence of spectral beam splitting on the temperature, maximum power and efficiency of a polycrystalline silicon cell under concentrated light. The PV cell was exposed to wavelengths ranging between 450 nm – 1000 nm. It was found that spectral beam splitting results in a temperature 11 °C lower than the PV cell that was exposed to the full spectrum after one hour.

Additionally, it was also found that spectral beam splitting improves the efficiency of the PV cell by 2.1% at 980 W·m<sup>-2</sup> and cell temperature of 25 °C. A study into the effect of light intensity on the efficiency showed that the efficiency increases between 580 W·m<sup>-2</sup> – 680 W·m<sup>-2</sup>, after which the efficiency decreases up to 1380 W·m<sup>-2</sup>. Furthermore, it was found that the reason for the decrease in the efficiency was the decrease in the fill factor which is caused by the decrease in the shunt resistance. A comparison between the PV cell under the filtered spectrum and the full spectrum, showed that the PV cell exhibits a similar trend in efficiency as light intensity increases. However, the efficiency difference is initially at approximately 3% between 580 W·m<sup>-2</sup> and 780 W·m<sup>-2</sup>, thereafter, the efficiency difference decreases to approximately 2 %.

Based on these results, it has been recommended that further research be carried out to understand how wavelengths influence the band gaps of PV cells as the light intensity increases.

Keywords: Photovoltaic effect, spectral beam-splitting, optical filters, I-V graphs, efficiency, polycrystalline silicon.

# Contents

Nomenclature	vii
Introduction	1
1. Theory.....	3
1.1 The solar spectrum.....	3
1.2 Photovoltaic (PV) cells .....	4
1.3 Modelling PV cells .....	5
1.3.1 I-V curve.....	6
1.4 Types of PV cells.....	7
1.5 Characterising PV cells.....	7
1.5.1 Photocurrent and quantum efficiency.....	7
1.5.2 PV cell efficiency .....	8
1.5.3 Dark Current and Open circuit voltage .....	8
1.5.4 Resistances .....	9
1.6 Factors influencing performance of PV cells .....	10
1.6.1 Spectral response (SR) .....	10
1.6.2 Cell temperature .....	11
1.6.3 Light intensity.....	12
1.7 Optical filters .....	13
1.7.1 Spectral beam splitting .....	13
1.7.2 Dichroic Filters.....	15
1.7.3 Thin film interference.....	16
1.7.4 Dielectric multilayer materials .....	17
1.7.5 Nanofluid based optical filters .....	18
1.7.6 Optical filters for photovoltaic applications.....	18
1.8 Concentrated Photovoltaic (CPV) systems.....	20
2. Model.....	22
2.1 Analytical-numerical approach model.....	23

2.2 Parameter adjustment (Light intensity and temperature).....	24
2.2.1 Photocurrent ( $I_{ph}$ ).....	24
2.2.2 Series resistance ( $R_s$ ).....	24
2.2.3 Shunt resistance ( $R_{sh}$ ).....	25
2.2.4 Saturation Current ( $I_o$ ).....	25
2.2.5 Diode Ideality Factor ( $n$ ).....	25
2.3 Modelling assumptions.....	25
2.4 Modelling results.....	26
3. Experimental Method.....	27
3.1 Apparatus.....	27
3.1.1 Solar Concentrator.....	27
3.1.2 Spectral beam splitter (Optical filter).....	27
3.1.3 Light intensity measurements.....	28
3.1.4 Generating a characteristic IV curve.....	29
3.1.5 External cooling.....	30
3.2 Experimental design.....	30
3.2.1 Influence of optical filter on the temperature of a PV cell (same light intensity).....	31
3.2.2 Quantifying the temperature change and efficiency of the PV cell for transmitted and reflected light.....	32
3.2.3 Influence of optical filter on the performance of a PV cell at constant temperature ...	33
3.2.4 Influence of optical filter on the performance of a PV cell with varying temperature	34
3.2.5 Influence of light intensity on the performance of a PV cell.....	34
4. Results and Discussion.....	36
4.1 Influence of the optical filter on the temperature of a PV cell (same light intensity).....	36
4.2 Quantifying the temperature change of the PV cell for transmitted and reflected light.....	37
4.3 Influence of spectral beam splitting on the performance of a PV cell at isothermal conditions.....	37
4.4 Influence of optical filter on the performance of a PV cell with varying temperature.....	39

4.5 Response of PV cells to transmitted and reflected wavelength at isothermal conditions.....	43
4.6 Influence of light intensity on the performance of a PV cell under the full solar spectrum...	44
4.7 Influence of light intensity on the performance of a PV cell under the filtered spectrum.....	47
5. Conclusions .....	50
6. Recommendations .....	52
7. References .....	53
8. Appendix .....	57
A. Optical filter (product specification).....	57
B. Model Code.....	57

## Nomenclature

$I_d$	Dark saturation current	A
$I_o$	Diode saturation current	A
$I_{oref}$	Diode saturation current (reference conditions)	A
$I_{ph}$	Photocurrent	A
$I_{phref}$	Photocurrent	A
$I_{sc}$	Short circuit current	A
$I_{scref}$	Short circuit current (reference conditions)	A
$I_{sc\_a}$	Short circuit current per unit area	$A \cdot m^{-2}$
$k$	Boltzmann constant	$A \cdot W$
$T_c$	Cell temperature	$^{\circ}C$
$T_{cref}$	Cell temperature	$^{\circ}C$
$V$	Cell output voltage	V
$I$	Cell output current	A
$P_{in}$	Power in	W
$P$	Power	P
$P_{max}$	Maximum power	W
$FF$	Fill factor	-
$I_{max}/I_m$	Current at maximum power	A
$V_{max}/V_m$	Voltage at maximum power	V
$h$	Plank's constant	-
$c$	Speed of light	$m \cdot s^{-1}$
$E$	Energy of photon	eV
$E_g$	Bandgap energy	eV
$n$	Diode ideality factor	-
$n_{ref}$	Diode ideality factor (reference conditions)	-
$R_s$	Series resistance	$\Omega$
$R_{sref}$	Series resistance	$\Omega$
$R_{sh}$	Shunt resistance	$\Omega$
$R_{shref}$	Shunt resistance	$\Omega$
$N_s$	Number of cells connected in series	-
$\theta$	Solar zenith angle	$^{\circ}$
$G$	Light intensity/irradiance	$W \cdot m^{-2}$

$G_{\text{ref}}$	Light intensity/irradiance (reference conditions)	$\text{W}\cdot\text{m}^{-2}$
$V_t$	Thermal Voltage	V
$\mu_{\text{sc}}$	Short circuit temperature coefficient	$\text{A}\cdot\text{K}^{-1}$
SR	Spectral response	$\text{A}\cdot\text{W}^{-1}$
QE	Quantum Efficiency	%
q	charge	C
$\eta$	Efficiency	%
$\lambda$	wavelength	nm



## Introduction

Efficient use of solar energy is a possible alternative to fossil fuels. The use of fossil fuels has proved to be unsustainable because of the greenhouse gases that are released during combustion. Moreover, fossil fuels are non-renewable resources. This means that they become depleted the more they are used.

The total world energy consumption in 2016 was approximately 17.72 TW (BP, 2017). This is very little contrary to 173,000 TW which is the estimated amount of solar energy received by earth from the sun every hour (Soulayman, 2017). Harvesting energy from solar radiation has the potential to meet the global energy demand (Mojiri *et al*, 2013). Solar thermal and photovoltaic power plants are two available technological platforms that use the sun's energy to produce heat and electricity efficiently. This makes them suitable for application in regions with high solar irradiance.

Currently photovoltaic (PV) cells have reached efficiencies of up to 46% in laboratory measurements (National Energy Research Laboratory (NREL), 2017). This because they are designed to capture a larger portion of the solar spectrum. Nevertheless, these high efficiency materials have very high manufacturing costs. Concentrated photovoltaic technology has the potential to reduce the overall cost of solar energy systems; if the optics used to concentrate the light are cheaper than the reduction in area of the cell that would be used to produce the same amount of electricity without concentrated sunlight.

Concentrated photovoltaic (CPV) technologies convert sunlight into electricity. However, unlike conventional photovoltaic systems, CPVs use lenses and curved mirrors to concentrate sunlight onto the photovoltaic cells. CPV cells work by increasing the number of photons from the light that come in contact with the PV cell and therefore increase the chances of electrons in the valence band overcoming the energy band gap to move to the conduction band. This means that more current can flow in a circuit.

CPV technology can be very suitable to produce electricity in parts of the world with high levels of solar irradiance. However, concentrating light onto a photovoltaic cell reduces the cell's efficiency. This is because, increasing the concentration of light increases the cell temperature. This heat can be removed by actively or passively cooling the PV cell which requires external mechanisms such as thermal fluids for very high temperatures. An alternative method is to decouple the heat from electricity by splitting the solar spectrum such that only the wavelengths that result in the production of electricity are incident on the PV cell. The advantage of the alternative is that the PV cell is not damaged due to high temperatures. Moreover, splitting the spectrum can improve the efficiency of the PV cell (Chendo, Jacobson & Osborn, 1987). Therefore, there is a need to carry out research to understand how PV cells behave under a spectrally split spectrum.

The objectives of this report are:

- To determine the influence of spectral beam splitting on the temperature of PV cells
- To determine if spectral beam splitting improves the efficiency of solar cells
- To compare the effect of light intensity on the efficiency for PV cells under a spectral beam splitter.

A short pass dichroic filter was used to expose a polycrystalline PV cell to wavelengths between 450 nm – 1000 nm of the solar spectrum. The characteristic I-V curve and the temperature of the PV cell was measured using a National Instruments (NI) DAQ module. Thereafter, a parameter extraction technique was used to determine the PV cell parameters which made it possible to determine the efficiency of the PV cell. Experiments were carried out to compare the effect of light intensity and temperature on the performance of the PV cell under a filtered solar spectrum to PV cells under the full solar spectrum.

# 1. Theory

## 1.1 The solar spectrum

Energy from the sun comprises electromagnetic waves that are distributed over a spectrum of varied wavelengths. The different forms of electromagnetic radiation include: gamma rays, x-rays, ultra-violet light, visible light, infrared light, microwaves and radio waves. The spectrum of the sun's solar irradiation can be represented by a black body at a temperature of 5778 K (Iqbal, 1983: 55) . This is illustrated in Figure 1.

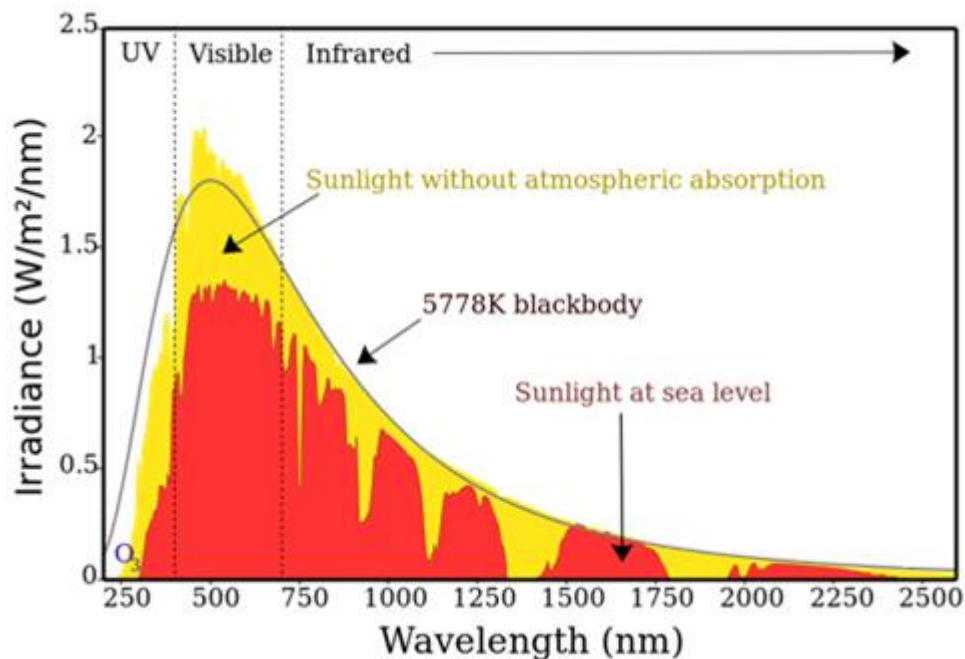


Figure 1: Solar spectrum showing the solar spectrum of the sun (Pagliaro, Palmisano & Ciriminna, 2008: 37).

When solar radiation is transmitted through the earth's atmosphere, it comes into contact with the atmospheric particles and therefore, is absorbed, reflected or refracted. This results in attenuation of light across the solar spectrum (Iqbal, 1983: 107). As can be seen from Figure 1, the atmosphere reduces the irradiance. Furthermore, we can also observe that that largest portion of the spectrum that reaches earth's surface is from the visible range.

Solar irradiation is the flux of energy per unit area measured in units of ( $W \cdot m^{-2}$ ). The total flux that is incident on a horizontal surface of the earth is referred to as the Global Horizontal Irradiance (GHI). The Direct Normal Irradiation (DNI), refers to radiation coming directly from the sun, normal to the horizontal surface. Finally, the Diffuse Horizontal Irradiance (DHI) is the flux reaching the earth's that has been

scattered by the atmosphere and the earth's surface. These three categories of irradiance can be correlated by:

$$\text{GHI} = \text{DNI} \times \cos(\theta) + \text{DHI} \quad (1)$$

where  $\theta$  is the zenith angle; the angle between the position of the sun and the plane parallel to the horizontal surface (Vignola, Michalsky & Stoffel, 2016: 23).

## 1.2 Photovoltaic (PV) cells

Photovoltaic cells otherwise referred to as solar cells, convert solar energy into electricity by a process called the photovoltaic effect. The photovoltaic effect is a process where light energy containing packets of energy called photons having a specific frequency or colour, excite electrons from the atoms of the material in ground state to higher energy levels where they can move freely. In photovoltaic devices, the excited electrons are fed into an external circuit (Nelson, 2003: 2).

Photovoltaic conversion depends primarily on the wavelength of the incident photons coming into contact with the photovoltaic material. This process is most efficient when the energy provided is equal to the band-gap energy. The band-gap energy is the energy difference between the conduction band and the valence band. For a PV cell to produce electricity, photons are required to excite an electron from the valence band into the conduction band. This results in a hole in the valence band. For this to occur all the momentum and all the energy must be conserved during transition of the electrons. The energy provided by the photon should enable the electron to overcome the band-gap energy (Green, 1982: 43).

Photons with energy less than the energy bandgap are usually dissipated as heat from the photovoltaic material. On the other hand photons with a larger energy than the band gap are partially used; the energy required by the energy bandgap is used and the excess energy is then dissipated as heat (Imenes & Mills, 2004).

In order for the PV cell to generate power, voltage and current need to be generated. The photovoltaic effect facilitates the generation of voltage. For this to occur, the positive and negative charges need to be separated. The basic device required to achieve this is a semiconductor with electronic asymmetry. This means that the semiconductor device should have one region with large electron densities (n-type) but small hole densities while the other region (p-type), will have small electron densities and large hole densities (Green, 1982: 62).

P-n junctions are used to achieve this. Additionally, the silicon p-n junction serves as a reference device for all solar cells (Sze, 1981: 798). P-n junctions are produced by doping the semiconductor materials. Increasing the electron density is referred to as n-type doping while increasing the number of holes is

called p-type doping. When the n-type and p-type semiconductor materials are brought into contact, the electrons from the p-type side tend to diffuse towards the n-type side and similarly leaving holes behind. This movement of electrons and holes leaves exposed charges on the atom's sites which are unable to move in the crystal lattice. An electric field forms between the exposed positive site for the n-type material and negative site for the p-type material. The region where the electric field is created is referred to as the depletion region. This is the region which causes the free carriers to go into the circuit. Free carriers are the holes and electrons that go into the circuit (Green, 1982: 63). Consequently, a potential difference develops from the electric field that is formed. Figure 2 is a schematic of a p-n junction.

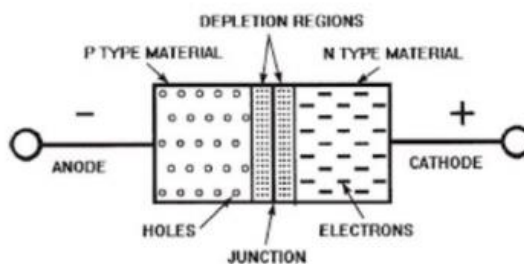


Figure 2: p-n junction

### 1.3 Modelling PV cells

The simplest model of a PV cell is a circuit shown on Figure 3.  $I_{ph}$  is the photo-generated current;  $I_d$  is the “dark” current flowing through the p-n junction;  $R_{sh}$  is the shunt resistance which accounts for energy losses in the circuit due to crystal defects and surface leakages along the edge of the cell, and  $R_s$  is the series resistance which accounts for the bulk resistance of the semiconductor material of which the cell is composed. It also accounts for ohmic losses from the front of the cell surface, and between the metal contacts in the PV cell (Green, 1982: 96).

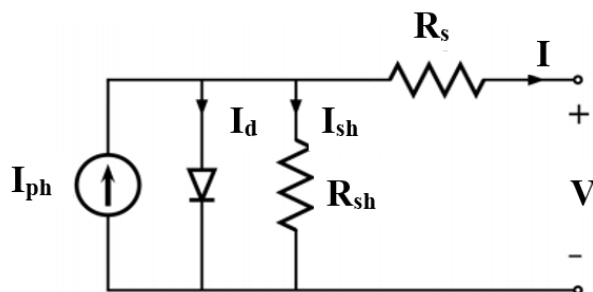


Figure 3: Model circuit of a PV cell

### 1.3.1 I-V curve

According to the circuit presented in Figure 3, the relationship between current and voltage can be expressed by the single diode ideal equation given by:

$$I = I_{ph} - I_0 \left[ \exp \left( \frac{q(V + IR_s)}{nN_s k T_c} \right) - 1 \right] - \frac{(V + IR_s)}{R_{sh}} \quad (2)$$

where  $I_{ph}$  is the light-generated current in amps,  $I_0$  is the cell saturation current in amps,  $n$  is an ideality factor,  $k$  is the Boltzmann's constant ( $1.3805 \times 10^{-23}$  N. m.  $K^{-1}$ ),  $N_s$  represents the number of PV cells connected in series,  $T_c$  is the cell temperature in kelvin (K),  $q$  is the electronic charge in coulombs ( $1.6 \times 10^{-19}$  C),  $R_s$  is the series resistance ( $\Omega$ ) and  $R_{sh}$  the shunt resistance ( $\Omega$ ). Plotting Equation 2 results in the I-V curve shown in Figure 4(a). Multiplying the current at each point on the I-V curve and plotting it against the voltage gives the P-V curve shown in Figure 4(b).

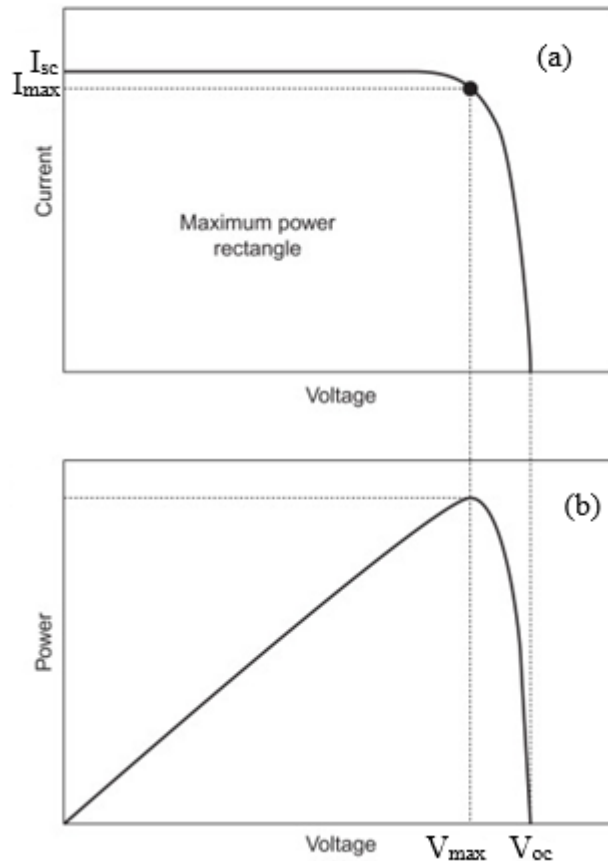


Figure 4: Characteristic I-V and P-V curve for a PV cell, for the ideal case  $I_{sc} = I_{ph}$  and the  $V_{oc}$  is defined by Equation 10.

## 1.4 Types of PV cells

Solar PV cells can be classified into first, second and third generation cells. First generation cells are made of crystalline silicon of which the commercially available cells are polycrystalline and monocrystalline silicon. The second-generation cells are the thin film solar cells which are made of cadmium telluride (CdTe), copper indium gallium selenide (CIGS) and amorphous silicon. The third generation of solar cells include a myriad of emerging PV cells, most of which are yet to be commercialised because they are still in the research and development stages. Third generation PV cells are mostly composed of organic materials. There is a lot of research invested into third generation PV cells due to low production costs compared to silicon PV cells which are commercially available (Gupta & Ballato, 2006: 8-4).

Monocrystalline and polycrystalline technology have the largest share of the PV market, accounting for 94 % of the solar PV market share (Fraunhofer Institute for Solar Energy Systems, 2017). This is because silicon is abundant, non-toxic and efficient (Gupta & Ballato, 2006: 8-4).

## 1.5 Characterising PV cells

### 1.5.1 Photocurrent and quantum efficiency

The current that is produced by a solar cell that is exposed to solar light depends on the light that is incident to the surface of the solar cell. The quantum efficiency (QE) or external quantum efficiency (EQE) of a solar cell relates the short circuit current density ( $I_{sc}$ ) to the power density that is incident to the surface of the solar cell. It is the ratio of the number of electron-hole pairs produced by a solar cell to the number of photons that come into contact with the solar cell surface (Klampafitis *et al*, 2009). In addition, it depends on the absorption coefficient of the device, the charge separation efficiency and the charge collection efficiency. It does not depend on the irradiated solar energy (Nelson, 2003: 8). The absorption coefficient quantifies how far into a material a photon can penetrate before it is absorbed (Rogalski, Adamiec & Rutkowski, 2000).

The relationship between photocurrent and quantum efficiency is given by:

$$I_{sc,a} = q \int_0^E G(E)QE(E)dE \quad (3)$$

where  $I_{sc,a}$  is in units of ( $\text{mA} \cdot \text{m}^{-2}$ ),  $q$  is the electronic charge in coulombs (C),  $G(E)$  is the spectral photon flux density in ( $\text{W} \cdot \text{m}^{-2}$ ),  $QE(E)$  is a dimensionless value (Nelson, 2003: 7-8).  $E$  is the energy of the photons on a unit area per unit time ( $\text{J} \cdot \text{m}^{-2}\text{s}^{-1}$ ).

Additionally, the quantum efficiency (QE) and the solar spectrum can be expressed as functions of the photon energy or the wavelength. They are related by:

$$E = \frac{hc}{\lambda} \quad (4)$$

Where E is the photon energy, h is Planck's constant, c is the speed of light in a vacuum in (m·s<sup>-1</sup>) and λ is the wavelength of light (m) (Nelson, 2003: 8).

### 1.5.2 PV cell efficiency

The efficiency of a solar cell is the ratio of the maximum power from the PV cell to the power that is incident to the solar cell. The efficiency of a solar cell is calculated by:

$$\eta = \frac{P_{\max}}{P_{\text{in}}} = \frac{I_{\max}V_{\max}}{P_{\text{in}}} \quad (5)$$

where P<sub>in</sub> is the power that is incident to the PV cell in Watts (W). These reported efficiencies are usually determined under standard test conditions for solar cells (illumination = 1000 W/m<sup>2</sup>, temperature = 25 °C and AM = 1.5).

The efficiency can also be expressed as a function of the incident power (P<sub>in</sub>), the open circuit voltage (V<sub>oc</sub>), short circuit current (I<sub>sc</sub>) and the fill factor (FF):

$$\eta = \frac{\text{FF } I_{\text{sc}}V_{\text{oc}}}{P_{\text{in}}} \quad (6)$$

This is based on the assumption that FF and V<sub>oc</sub> are not wavelength dependent (Overstraeten & Mertens, 1986). Additionally, it is also important to note that the fill factor is influenced by the series resistance (R<sub>s</sub>) and the shunt resistance (R<sub>sh</sub>) as can be seen from Figure 6.

### 1.5.3 Dark Current and Open circuit voltage

When solar circuits have a load, a potential difference develops across the solar cell. This results in the generation of current which acts in the reverse direction to the photo current. This reverse current is referred to as the dark current; it flows in the circuit in the dark under bias (Nelson, 2003: 9). The difference between the two flows results in the short circuit. For an ideal diode, the dark current (I<sub>d</sub>) is given by:

$$I_d = I_o \left( e^{qV_t/kT} - 1 \right) \quad (7)$$

I<sub>o</sub> is the saturation current in amps (A), k is the Boltzmann's constant (1.3805 x 10<sup>-23</sup> N · m · K<sup>-1</sup>), q is the electronic charge in coulombs (1.6 x 10<sup>-19</sup> C), T is the module temperature in Kelvin (K), and V<sub>t</sub> is the voltage across the diode. The overall current-voltage behaviour can be estimated as the sum of the short



circuit current and dark current. This is illustrated in Figure 5. The sign convention for current and voltage used is such that the photocurrent is positive (Nelson, 2003: 10). Figure 5 depicts the characteristic I-V graph for PV cells under solar irradiation and in the absence of irradiation.

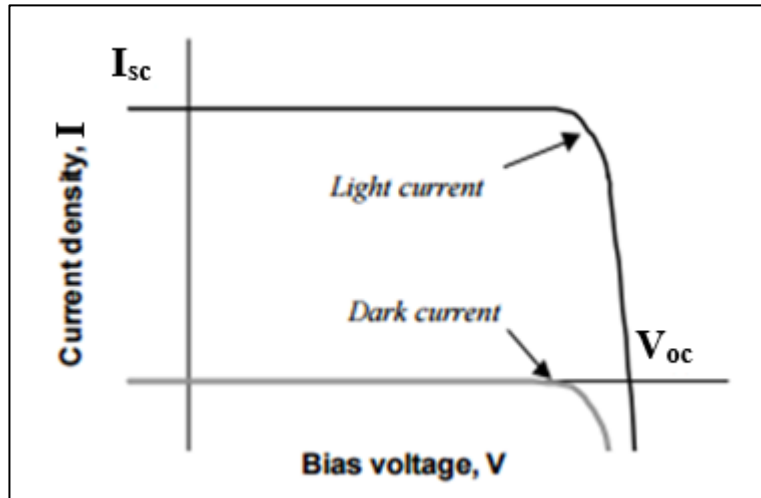


Figure 5: Current-Voltage behaviour of an ideal diode in the light and in the dark (Nelson, 2003: 10)

The net current density of a solar cell is given by:

$$I = I_{sc} - I_d \quad (8)$$

Equation 7 can be substituted into Equation 8, resulting in:

$$I = I_{sc} - I_o \left( e^{qV_t/kT} - 1 \right) \quad (9)$$

where  $I_{sc}$  is the photocurrent in amps (A).

At the point where the difference between the short circuit current and the dark current is zero i.e. when no current is flowing through the circuit, the resulting voltage is referred to as the open circuit voltage. The open circuit voltage can then be derived using Equation 9 as:

$$V_{oc} = \frac{kT}{q} \ln \left( \frac{I_{sc}}{I_o} + 1 \right) \quad (10)$$

#### 1.5.4 Resistances

The shunt resistance and the series resistance of solar cells influence the characteristic current-voltage graph of solar cells. These resistances can be referred to as parasitic resistances. The influence of these resistances on the characteristic I-V graph are shown on Figure 6. For both Figure 6(a) and Figure 6(b), the outer curve has  $R_s = 0$  and  $R_{sh} = \infty$ . It can be seen that increasing the series resistance results in a decrease in maximum power. On the other hand, decreasing the shunt resistance also decreases the maximum power of the PV cell (Nelson, 2003: 14).

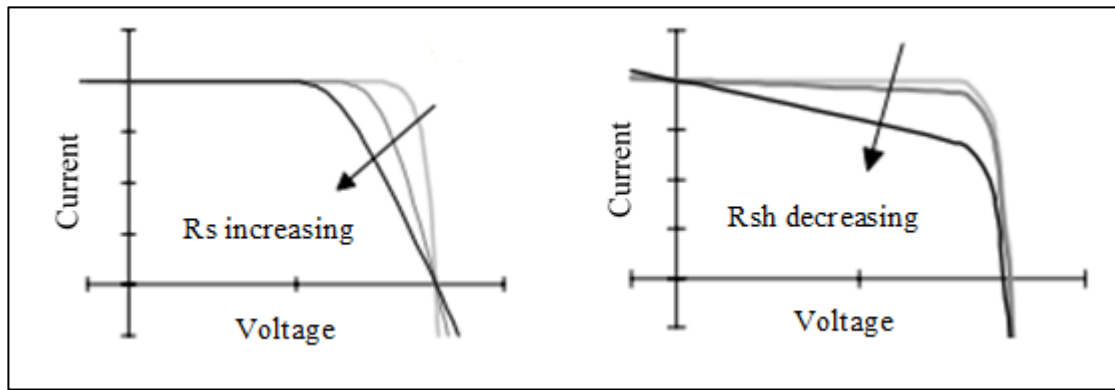


Figure 6: a) Influence of series resistance on the characteristic I-V graph b) Influence of shunt resistance on the I-V graph (Nelson, 2003: 14)

At low voltages, the effective resistance of the PV cell is high, therefore the effect of resistances in parallel (shunt resistances) is also high. Since the effective resistance is higher, then current will leak through alternative paths of least resistance.

## 1.6 Factors influencing performance of PV cells

The performance of PV cells is affected by the cell temperature, light intensity, the solar spectrum and the PV cell material.

### 1.6.1 Spectral response (SR)

The spectral response determines the performance of any solar cell over the solar spectrum. It is the current ( $I$ ) generated by a PV cell exposed to radiation with power,  $P_{in}$ . It is given by:

$$SR = \frac{I}{P_{in}} \quad (11)$$

where  $I$  (A) is the current generated at a particular wavelength, and  $P_{in}$  is the power (W) of the incident radiation at a particular wavelength.

Spectral response is a material dependent parameter which depends on the bandgap energy of the material. Figure 7 shows the normalised spectral response curve for a polycrystalline silicon PV cell exposed to a monochromatic light source. When we look at spectral response for silicon PV cells, we see that a spectral response is produced in the range of 300 nm - 1200 nm. Wavelengths outside this range do not result in the production of electricity in the PV cell.

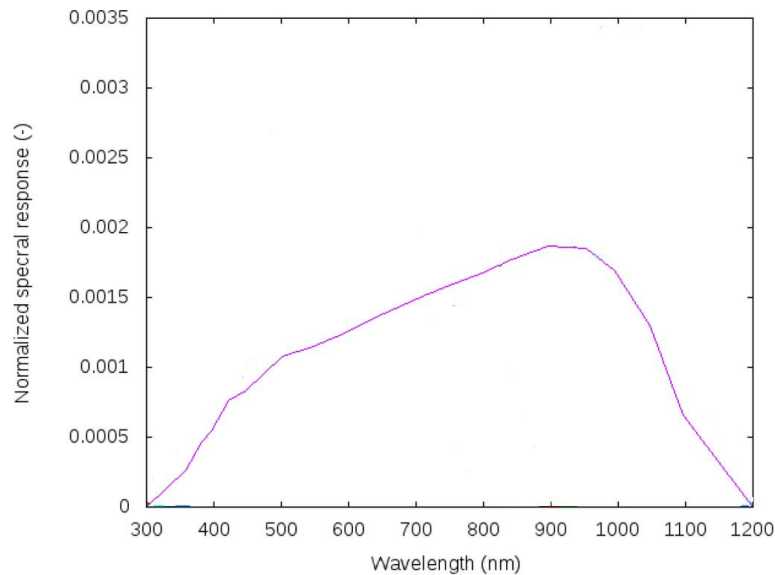


Figure 7: Normalised spectral response data for a crystalline silicon cell (Amillo *et al*, 2015)

Additionally, the bandgap energy for silicon, 1.12 eV, is equal to a photon of wavelength 1127 nm. Therefore, photons with wavelengths longer than this value, are not able to provide enough energy for the electron to move from the valence band to the conduction band. On the other hand wavelengths shorter than the 1127 nm have excess energy which is dissipated as heat at the cell junction (Mojiri *et al*, 2013).

Ideally, PV cells should only be exposed to wavelengths that do not dissipate energy as heat. This is because heat reduces the efficiency of the PV cell. The best range to achieve this, is between 700 nm – 1100 nm because they have energy that is close to the bandgap (Mojiri *et al*, 2013). Nevertheless, wavelengths outside the specified range also result in the generation of electricity which means that if the silicon cell is only exposed to wavelengths between 700 nm – 1000 nm at a specific light intensity, then the efficiency increases, but the power decreases.

### 1.6.2 Cell temperature

For silicon PV cells, the efficiency decreases as the cell temperature increases. This is mainly due to the influence of temperature on the parasitic resistances which influences the fill factor. The  $R_s$  increases as the temperature increases (Bensalem & Chegaar, 2013) . This reduces the fill factor. On the other hand, the  $R_{sh}$  decreases with increased cell temperature (Bensalem & Chegaar, 2013) which also reduces the fill factor.

For the other parameters, the temperature has a greater impact on the open circuit voltage ( $V_{oc}$ ) than on the short circuit current ( $I_{sc}$ ) (Green, 1982: 91-92). The short circuit current ( $I_{sc}$ ) increases slightly as cell temperature increases (Singh *et al*, 2008, Wysocki & Rappaport, 1960, Cuce, Cuce & Bali, 2013). The increase in the short circuit current is because the cell has an increased light absorption since the bandgaps

become smaller as the temperature increases. This means that it is able to convert more of the wavelengths into electricity (Green, 1982: 91).

### 1.6.3 Light intensity

When we look at light intensity, we consider the number of photons that are incident to the surface of the PV cell per unit area. Increasing the light intensity increases the number of photons incident to the cell. Therefore, more energy is available to enable free carriers to go into the circuit resulting in more power.

For polycrystalline silicon PV cells, light intensity significantly influences the cell's efficiency. The influence of light intensity on the PV cell depends on the incident radiation's effect on the PV cell's fill factor, short circuit current and open circuit voltage as can be seen from Equation 6. The open circuit voltage is logarithmically dependent on the light intensity as is seen in Equation 10, while the short circuit current has a linear relationship with the light intensity (Chegaar *et al*, 2013).

It has also been discussed that the fill factor is influenced by parasitic resistances. At low light intensities, less current flows through the circuit meaning that any losses of current via the shunt pathway has significant impacts on the PV cell.

Figure 8 provides an indication of the expected trend in efficiency of polycrystalline PV cells with increased light intensity at low voltages. The experiments were both carried out in a xenon solar simulator. Nevertheless, the polycrystalline PV cells were not fabricated in the same way nor were the characteristic I-V curves generated using the same type of equipment. However, we can see that there is small increase efficiency at low light intensities, intensity  $< 1000 \text{ W}\cdot\text{m}^{-2}$ , after which the efficiency is observed to decrease.

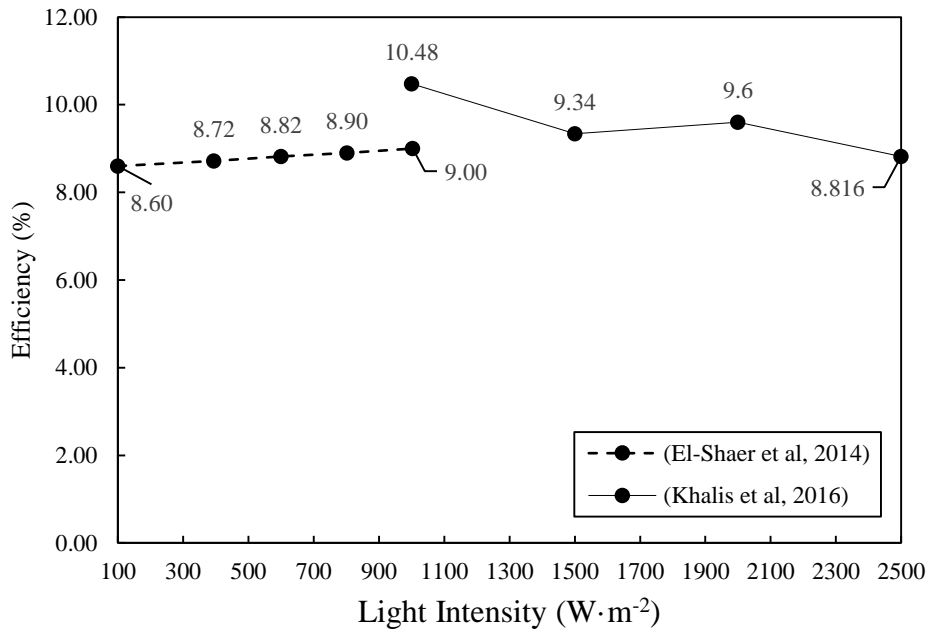


Figure 8: Influence of light intensity on polycrystalline silicon cells at  $25\text{ }^{\circ}\text{C}$ :  $100\text{ W}\cdot\text{m}^{-2} - 1000\text{ W}\cdot\text{m}^{-2}$  (El-Shaer, Tadros & Khalifa, 2014) and  $1000\text{ W}\cdot\text{m}^{-2} - 2500\text{ W}\cdot\text{m}^{-2}$  (Khalis *et al*, 2016)

To explain the initial small increase in efficiency as between  $100\text{ W}\cdot\text{m}^{-2} - 1000\text{ W}\cdot\text{m}^{-2}$ , the cell efficiency increases with light intensity because the short circuit current ( $I_{sc}$ ) increases significantly and linearly as light intensity increases. It is important to note that this phenomenon is only possible if the temperature of the solar cell remains unchanged as light intensity is increased (Chegaar *et al*, 2013). On the other hand, it has also been shown the open circuit voltage increases only slightly and exponentially with increased light intensity as seen in Equation 10.

The decrease in efficiency between  $1000\text{ W}\cdot\text{m}^{-2}$  to  $2500\text{ W}\cdot\text{m}^{-2}$  is attributed to the fact that the parasitic resistances ( $R_s$  and  $R_{sh}$ ) begin to influence the performance of PV cells. This reduces the fill factor which reduces the efficiency of the PV cell (Khalis *et al*, 2016).

## 1.7 Optical filters

### 1.7.1 Spectral beam splitting

Spectral beam splitting refers to the removal/filtering of wavelengths over a particular range of the solar spectrum while only allowing a particular range of wavelengths to be transmitted. For PV applications, spectral beam splitting can be applied to reduce heating due to wavelengths with energy lower than or greater than the bandgap energy.

At high concentration levels, additional cooling of the PV cells is required even in a beam splitting system. The photovoltaic band can be transmitted to the solar cells, with the balance reflected to a photothermal system; this type of filter is called a bandpass filter.

Alternatively, the PV band can be reflected; this is a bandstop or minus filter configuration. Whether the bandpass or bandstop approach will be chosen will depend not only on the optical performance of the filter, but also on how the overall system design is affected. For example, since photothermal systems involving heat-transfer fluids are generally heavier than PV cells, the bandstop approach permits the photothermal component to be placed under the beam splitter and to suspend the lighter solar cells higher up (Imenes & Mills, 2004).

The ideal spectral characteristics of the beam splitting filter would be a perfect square wave as shown in Figure 9 (Imenes & Mills, 2004). A sharp transition between the transmissive and reflective regions is observed. The actual spectral characteristics will primarily depend on the materials used in addition to their thickness in the stacked filter. The objective function used to optimise the filter's transmittance and reflectance properties will depend on how the useful output energy is evaluated; in terms of high-quality electric energy, or whether it is combined with low-quality thermal energy.

Spectral beam splitters in hybrid PV/thermal systems have been shown to have many benefits because of how effectively the solar energy is used to produce electricity as well as how the heat is used (Osborn *et al*, 1986b). Nevertheless, the authors have also emphasised the need for economic evaluations including the extra cost of the beam splitter in order to assess the usefulness of the combined system. Arguments supporting the use of concentrated solar radiation have shown that the energy payback period can be reduced compared to having only commercial PV cells to produce electricity (Mojiri *et al*, 2013).

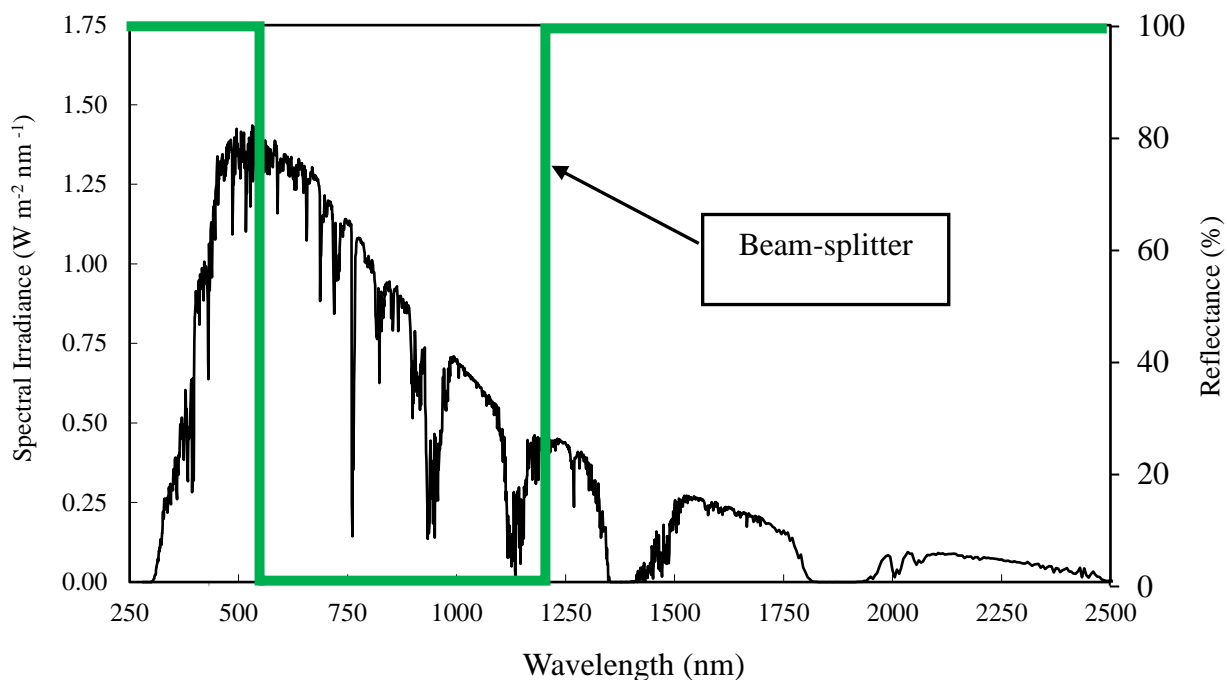


Figure 9: Graph showing the reflectance of an ideal beam splitter on an Air Mass (A.M) 1.5D solar spectrum (Imenes & Mills, 2004).

In spectral beam splitting applications, filters formed using thin-film dielectrics can be tuned to transmit a specific spectral band while reflecting another. Hot mirrors are an example of commercial available beam splitters; passing visible light while reflecting infrared. Moreover, spectral beam splitting allows the use of different, single-junction devices. This eliminates the fabrication challenges that come with lattice matching and tunnel junctions for multi-junction cells (Karp, 2008).

The factors that need to be considered when selecting beam splitters include (DeSandre *et al*, 1985): Optical performance; how a bandpass filter and a bandstop filter affects the overall system design; the ease of manufacture; minimum absorption of photons; material durability at high temperatures and rapid temperature changes.

Proposed spectral beam splitting techniques that have been used to improve PV cell efficiencies include: transmissive and reflective filtering methods, refractive and absorptive methods, luminescent filtering methods, and holographic filtering methods (Imenes & Mills, 2004).

### 1.7.2 Dichroic Filters

Dichroic filters also referred to as thin-film filters or interference filters are highly accurate colour filters that are designed to selectively pass light within a specific wavelength range

while reflecting the other wavelengths of light. They are composed of thin layers, ranging from a few nanometres to hundreds of nanometres in thickness, of non-absorbing dielectric materials with high refractive index. The dielectric materials are deposited on a transparent substrate to achieve the desired spectral splitting optical properties. Figure 10 depicts how thin-film wave interference filters work. They use a method called thin-film interference to split the wave spectra. The optical properties of the interference filters depend on the refractive index and thickness of each layer; the number of layers and how the layers are arranged (Osborn *et al*, 1986a).

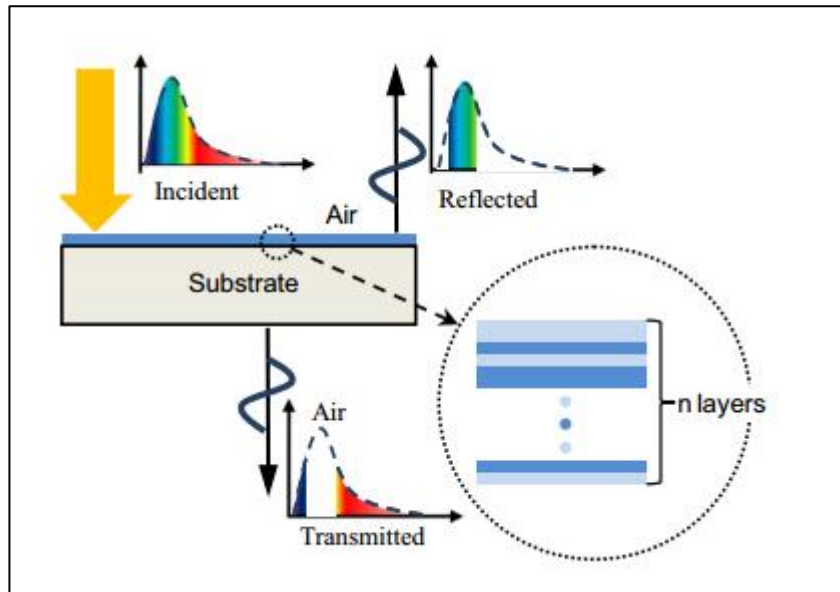


Figure 10: Illustration of spectral splitting using a thin-film interference filter (Mojiri *et al*, 2013)

### 1.7.3 Thin film interference

Interference filters are used in preference to other types of wavelength-selecting devices such as prism and grating monochromators. This is because of their light weight and mechanical stability. However, the major advantage of thin-film filters is the significant increase in the potential grasp of energy contrary to dispersive systems (MacLeod & Macleod, 2010: 540).

Thin film filters use the concept of the Fabry-Perot interferometer to achieve beam splitting. The interferometer has had a profound influence on the development of thin-film optics. It belongs to a group of interferometers referred to as multiple-beam interferometers because a large number of beams are involved in the interference (MacLeod & Macleod, 2010: 179).

A Fabry-Perot interferometer consists of two mirrors that can be flat or concave separated by a distance ( $L$ ) and aligned so that they are parallel to a very high degree of accuracy. The separation is usually maintained by a spacer ring that is composed of Invar or quartz. The setup consists of two plates and a



spacer is known as an etalon. The inner surfaces of the two plates are usually coated to improve their reflectance (Hernandez, 1988: 1).

Fabry-Perot interferometers use the multiple reflections between the parallel surfaces. A portion of the light is transmitted every time light reaches the second surface. This in turn results in many offset beams which can interact with each other, producing interference fringes. Figure 11 shows a schematic of the Fabry-Perot interferometer. The lens is used to project the fringes onto a scanning surface.

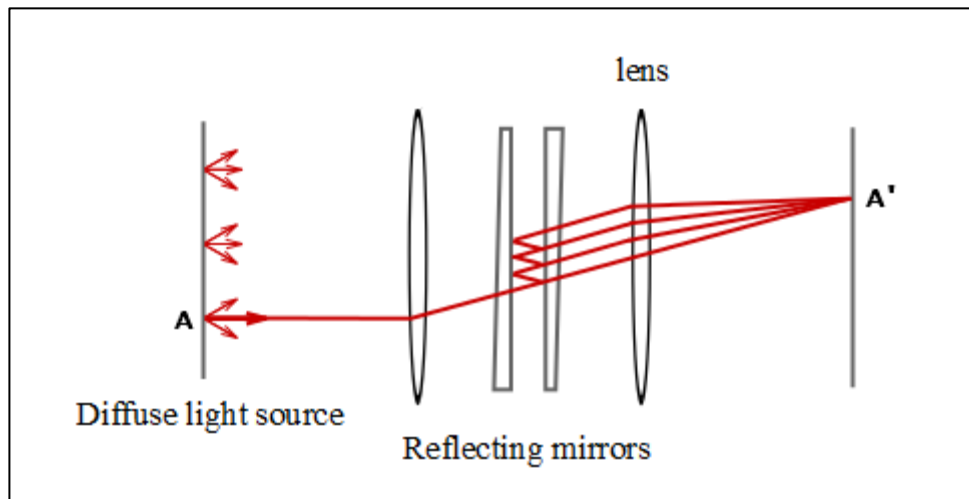


Figure 11: Schematic of a Fabry-Perot interferometer (Arrasmith, 2015: 673)

It is only specific wavelengths that will resonate in the cavity. Once this requirement is met, light at these wavelengths will accumulate in the spacing and can then be transmitted through the back end (Hernandez, 1988: 1).

#### 1.7.4 Dielectric multilayer materials

Metal reflecting layered coatings suffer from a considerable absorption loss when they are irradiated with solar energy. A possible solution to minimise energy loss through absorption for opaque metal coating, is to increase the reflectance by adding dielectric layers. Although this reduces the absorbance, transmittance remains effectively zero. For high-reflecting coatings which must not absorb any energy, all-dielectric multilayers are required (MacLeod & Macleod, 2010: 179).

An all-dielectric multilayer filter provides two main advantages for beam splitting applications: it undergoes minimum absorption, and it has highly adjustable filter spectral characteristics which can be altered by cautiously positioning the band-limited transmitted (or reflected) region.

Usually, an optical multilayer interference filter is lodged on a high quality, low absorption glass material such as fused quartz or borosilicate. This is because the range at which wavelengths are transmitted for

fused quartz and borosilicate are applicable to the spectral range of solar irradiation; ultraviolet (UV) is around 300-350 nm and in the infrared (IR) around 3000 nm.

Absorption within the transmission range (350-3000 nm) is very low i.e. 1-2% depending on the material and thickness of the glass layer (Imenes & Mills, 2004). The deposition technique and materials applied to the dielectric multilayer coating deposited on the glass substrate, could also result in some absorption loss. However, it is usually very small.

### **1.7.5 Nanofluid based optical filters**

Nanofluids based optical filter are an emerging method that present a great opportunity for spectral beam splitting because they can be used as both a spectral beam splitter and a heat transfer fluid (Otanicar, Taylor & Telang, 2013). This is especially practical to hybrid systems which capture both wavelengths for electric and thermal applications. Nanofluid optical filters are suspensions that are made by adding nanoparticles into fluids such as water, oil or glycol (Otanicar *et al*, 2010). The physical properties of the particles influence the ability of the nanofluid to absorb specific wavelengths making them suitable for transmitting desired wavelengths. Nevertheless, there are challenges associated with the development of homogenised suspensions, developing smaller sized particles (<50nm), and maintaining stable optical properties at high temperatures (Stanley, Morjiri & Rosengarten, 2016).

### **1.7.6 Optical filters for photovoltaic applications**

Attempts have been made to design different spectrally selective beam splitters to improve overall efficiency of photovoltaic cells. One experiment investigated three types of bandpass filters and two types of bandstop filters (DeSandre *et al*, 1985).

The three types of bandpass filters included: symmetric period filters which were composed of longwave-pass and shortwave-pass filters, induced-transmission filters which had two or more alternating high-index and low-index quarterwave layers, and metal-dielectric filter whose design is based on the Fabry-Perot Interferometer.

Broadband reflectance filters and optical minus filters were the two bandstop filters that were tested. Broadband reflectance filters are high reflectance filters consisting of alternating high-low stacks that are centered at a specified wavelength. On the other hand, optical minus filters operate by removing one wavelength band from a spectrum. This can be illustrated using a spectrum consisting of wavelengths,  $\lambda_1$  to  $\lambda_4$  referred to as the free filter range. For minus filters, the transmittance will be 100 % from  $\lambda_1$  to  $\lambda_2$ , 0% from  $\lambda_2$  to  $\lambda_3$ , and 100% again from  $\lambda_3$  to  $\lambda_4$ . The wavelength region  $\lambda_2$  to  $\lambda_3$  is called the rejection band (Thelen, 1970).

It was found that optical minus filters presented the best beam splitting results conveying high spectral performance and minimum absorption of the solar energy. Osborn *et al* (1986), also went further to investigate the application of optical minus filters for PV-thermal hybrid solar energy conversion systems. The experimental set-up is shown on Figure 12.

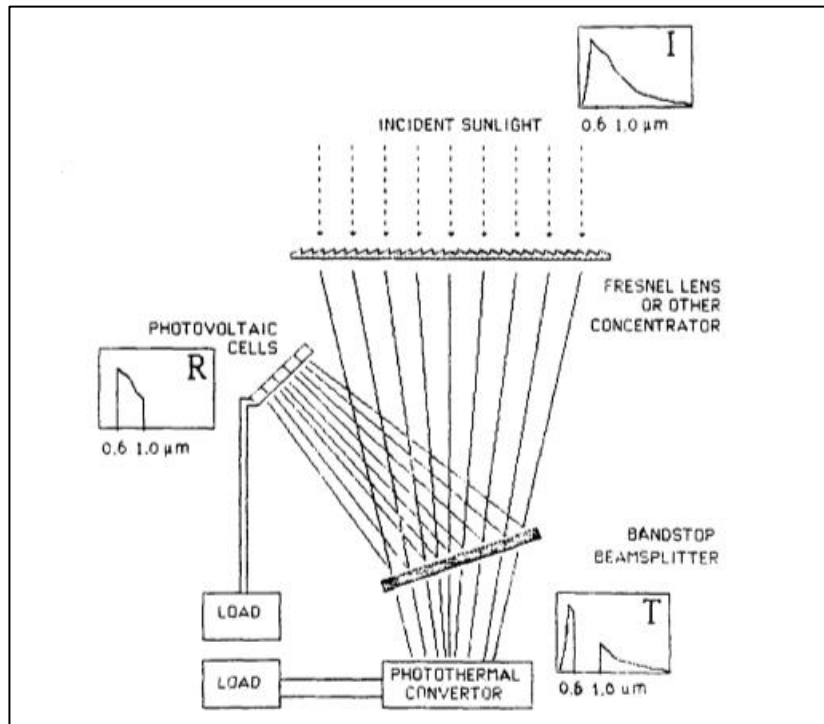


Figure 12: Hybrid solar energy conversion system using the optical minus filter system (Osborn *et al*, 1986a)

The designed filter significantly reflected wavelengths ranging from 0.68  $\mu\text{m}$  to 0.95  $\mu\text{m}$ . The spectral performance of the filter is shown on Figure 13.

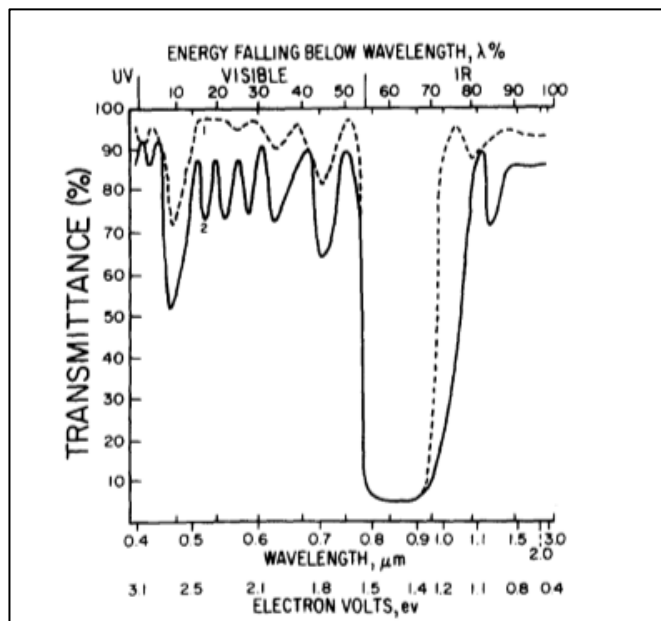


Figure 13: Spectral performance of the optical minus filter used by Osborn *et al* (1986).

Curve 1: expected/calculated results, Curve 2: Measured

### 1.8 Concentrated Photovoltaic (CPV) systems

Concentrated photovoltaic systems are systems that use cost-efficient concentrating optics to significantly reduce the cell area required by photovoltaic cell. This in turn, can potentially reduce the levelised cost of electricity (LCOE) allowing CPV systems to compete with concentrated solar power and conventional flat-plate PV technology in areas that are known to have high direct normal irradiance (DNI) (Kost *et al*, 2013).

CPV systems are differentiated based on the concentration factors as indicated in Table 1. In high concentration PV (HCPV) systems, a concentration factor ranging between 300× to 1000× is focused onto a small area using multi-junction solar cells. Low concentration PV (LCPV) systems mainly use crystalline (c-Si) solar cells and single axis tracking. Tracking systems are used to ensure that the CPV system utilises a large amount of the solar energy throughout the day. The concentration of sunlight onto PV cells can be carried out using Fresnel lenses or parabolic dish reflectors. CPV systems also usually have a finned heat sink to dissipate the concentrated heat from sunlight (Khartchenko & Kharchenko, 2013).

Table 1: Characteristics of different CPV systems based on concentration factors (Kost *et al*, 2013)

Concentration type	Typical Concentration ratio	Tracking	Type of Converter
High Concentration PV (HCPV)	300-1000	Two-axis	III-V multi-junction solar cells
Low Concentration PV (LCPV)	< 100	One or two-axis	c-Si or other cells

CPV technology promises a myriad of benefits to the energy industry: a smaller land area is required which provides land for other applications such as agriculture; CPV technology can also be applied to roof-tops of urban areas; stable energy production is available throughout the day; there is a low energy payback period, and CPV technology has a great potential to improve the balance of system (BOS) costs (Kost *et al*, 2013). Nevertheless, it also faces challenges such as lack of technology standardisation, additional optical losses and a need for a reliable, affordable and accurate tracking system.

## 2. Model

To model the polycrystalline PV cell for this project, the single diode model with the extraction of five parameters ( $I_{ph}$ ,  $I_o$ ,  $R_s$ ,  $R_{sh}$  and  $nN_{th}V_t$ ) was used for characterisation. The single diode equation provides relatively accurate results with simple calculation (de Blas *et al*, 2002). Furthermore, it is the most commonly used method in literature (Humada *et al*, 2016). These parameters were extracted at  $980 \text{ W}\cdot\text{m}^{-2}$  and  $25^\circ\text{C}$  cell temperature which is close to standard conditions. This is because most PV cell parameters are available at standard conditions. The parameter extraction was done using the  $V_{oc}$ ,  $I_{sc}$ ,  $I_{max}$  and  $V_{max}$  which were obtained from the characteristic I- V curve.

The analytical-numerical approach developed by Hejri *et al* (2016) was used to determine the five parameters of the PV cell at reference conditions. The parameters could then be adjusted using available correlations for temperature and light intensity. A schematic of the procedure is shown in Figure 14.

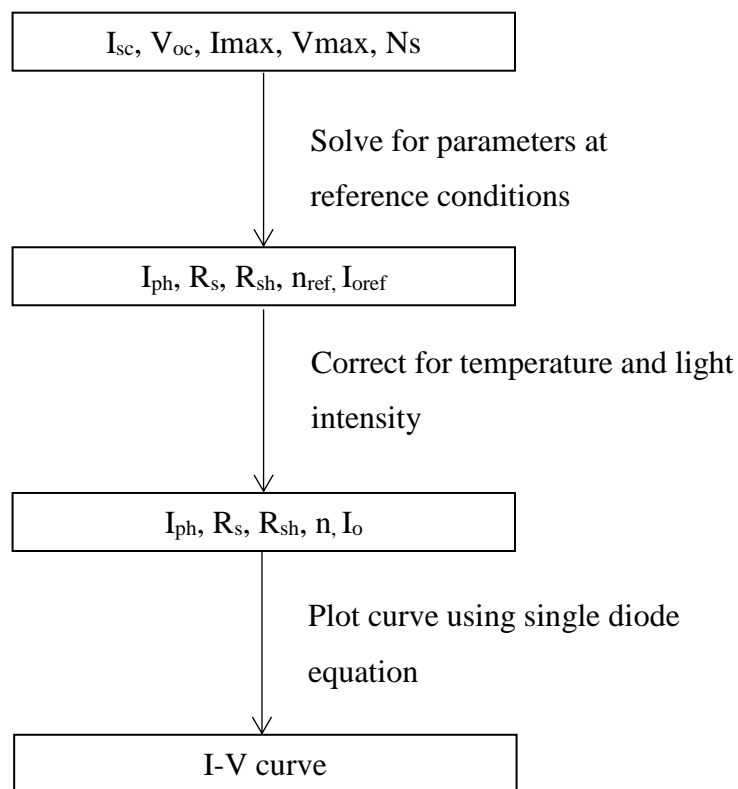


Figure 14: Schematic for obtaining the I-V curve using experimental data at reference conditions.

## 2.1 Analytical-numerical approach model

The five parameters to be determined are;  $I_{ph}$ ,  $I_o$ ,  $R_s$ ,  $R_{sh}$  and  $n$ . To be able to solve this, we need five independent equations. The reference condition for the calculations was  $980 \text{ W}\cdot\text{m}^{-2}$  and  $25^\circ\text{C}$  cell temperature. These conditions were chosen because the pyranometer used for experimentation could only be used with certainty up to  $1000 \text{ W}\cdot\text{m}^{-2}$ . To solve for the remaining terms, the boundary conditions are required. The following boundary conditions are used (Hejri *et al*, 2016):

$$V = V_{oc}, I = 0 \quad (12)$$

$$V = 0, I = I_{sc} \quad (13)$$

$$V = V_{max}, I = I_{max} \quad (14)$$

$$I = I_{sc} \text{ and } V = 0, \frac{dI}{dV} = -\frac{1}{R_{sh}} \quad (15)$$

Using the derivation method presented by Hejri *et al* (2016), the following independent equations are derived:

$$\frac{I_m}{V_m} = \frac{1}{nNsV_t} \left(1 - R_s \frac{I_m}{V_m}\right) \left(\frac{-V_{oc} + R_s + R_{sh}I_{sc}}{R_{sh}}\right) \exp\left(\frac{V_m - V_{oc} + R_s I_m}{nNsV_t}\right) - \frac{1}{R_{sh}} \left(1 - R_s \frac{I_m}{V_m}\right) \quad (16)$$

$$I_{sc} = I_o \left[ \exp\left(\frac{V_{oc}}{nNsV_t}\right) - \exp\left(\frac{R_s I_{sc}}{nNsV_t}\right) \right] + \frac{V_{oc} - R_s I_{sc}}{nNsV_t} \quad (17)$$

$$I_m \left(1 + \frac{R_s}{R_{sh}}\right) = I_o \left[ \exp\left(\frac{V_{oc}}{nNsV_t}\right) - \exp\left(\frac{V_{oc} + R_s I_m}{nNsV_t}\right) \right] + \frac{V_{oc} - V_m}{nNsV_t} \quad (18)$$

$$-\frac{R_s}{R_{sh}} + (R_{sh} - R_s) \exp\left(\frac{R_s I_{sc}}{nNsV_t}\right) = 0 \quad (19)$$

These equations can then be solved numerically via the Newton-Raphson method. Nevertheless, the biggest challenge with solving these equations is the saturation current value ( $I_o$ ). This is because the value is very small and so the iteration may not converge to a sensible solution (Hejri *et al*, 2016). To help prevent this from happening, the  $I_o$  is eliminated from the above equation by using the approximation that  $\exp(V_{oc}/V_t) \gg \exp(R_s I_{sc}/V_t)$  (Phang, Chander & Philips, 1984). The only unknowns will now be  $R_s$ ,  $R_{sh}$  and  $n$ .  $I_o$  can then be calculated using Equation 16, 17 or 18.

$$\frac{I_m}{V_m} - \frac{1}{nNsV_t} \left(1 - R_s \frac{I_m}{V_m}\right) \left(\frac{-V_{oc} + R_s + R_{sh} I_{sc}}{R_{sh}}\right) \exp\left(\frac{V_m - V_{oc} + R_s I_m}{nNsV_t}\right) - \frac{1}{R_{sh}} \left(1 - R_s \frac{I_m}{V_m}\right) = 0 \quad (20)$$

$$-I_m \left(1 + \frac{R_s}{R_{sh}}\right) + \left(\frac{-V_{oc} + (R_s + R_{sh}) I_{sc}}{R_{sh}}\right) \left[1 - \exp\left(\frac{V_m - V_{oc} + R_s I_m}{nNsV_t}\right)\right] + \frac{V_{oc} - V_m}{R_{sh}} = 0 \quad (21)$$

$$\frac{R_s}{R_{sh}} + \frac{R_{sh} - R_s}{nNsV_t} + \left(\frac{-V_{oc} + (R_s + R_{sh}) I_{sc}}{R_{sh}}\right) \exp\left(\frac{R_s I_{sc} - V_{oc}}{nNsV_t}\right) = 0 \quad (22)$$

Additionally, at the reference conditions, the photocurrent ( $I_{ph}$ ) is calculated by assuming that at the reference conditions,  $I_{ph} = I_{sc}$  (De Soto, Klein & Beckman, 2006).

## 2.2 Parameter adjustment (Light intensity and temperature)

### 2.2.1 Photocurrent ( $I_{ph}$ )

The photocurrent ( $I_{ph}$ ) depends on the incident light intensity and the cell temperature which can be calculated by:

$$I_{ph} = \frac{G}{G_{ref}} (I_{phref} + \mu_{sc} * (T_c - T_{cref})) \quad (23)$$

where  $I_{phref}$  is the photocurrent at the reference conditions,  $T_c$  is the temperature of the cell,  $T_{cref}$  is the temperature of the cell at reference conditions,  $G$  is the light intensity incident on the PV cell,  $G_{ref}$  is the light intensity incident on the cell at the reference conditions. Additionally,  $\mu_{sc}$  is the coefficient of temperature that is provided by the PV cell manufacturer (Bellia, Youcef & Fatima, 2014). The  $I_{phref}$  is assumed to be equal to the  $I_{sc}$  at the reference conditions (Bellia *et al*, 2014).

### 2.2.2 Series resistance ( $R_s$ )

The series resistance has a small effect on the I-V curve and so although there are correlations that can be used, it is assumed constant (De Soto *et al*, 2006).



### 2.2.3 Shunt resistance ( $R_{sh}$ )

The shunt resistance influences the gradient of the I-V curve at the short circuit point. It is affected largely by the incident solar radiation (De Soto *et al*, 2006). Therefore,  $R_{sh}$  is given by:

$$R_{sh} = \frac{G}{G_{ref}} R_{shref} \quad (24)$$

### 2.2.4 Saturation Current ( $I_o$ )

The saturation current is temperature dependent and can be estimated using the equation below (De Soto *et al*, 2006):

$$\frac{I_o}{I_{oref}} = \left[ \frac{T_c}{T_{cref}} \right]^3 \exp \left[ \frac{qE_g}{nk} \left( \frac{1}{T_{cref}} - \frac{1}{T_c} \right) \right] \quad (25)$$

where  $E_g$  is the bandgap energy at the cell temperature in eV,  $I_o$  is the diode saturation current in amps (A),  $k$  is the Boltzmann's constant ( $1.3805 \times 10^{-23} \text{ N} \cdot \text{m} \cdot \text{K}^{-1}$ ),  $q$  is the electronic charge in Coulombs ( $1.6 \times 10^{-19} \text{ C}$ ) and  $T_c$  is the cell temperature in Kelvin (K).

### 2.2.5 Diode Ideality Factor ( $n$ )

The diode ideality factor can be assumed to be linearly dependent on temperature and can be estimated by (De Soto *et al*, 2006):

$$\frac{n}{n_{ref}} = \frac{T_c}{T_{cref}} \quad (26)$$

where  $T_c$  is the temperature of the PV cell in Kelvin (K) and  $n$  is the diode ideality factor.

## 2.3 Modelling assumptions

In order to use the described model for the PV cell, the following assumptions were made:

- $\mu_{sc}$  was assumed to be negligible because temperature has a more significant effect on the open circuit voltage than on the short circuit current (Green, 1982: 91).
- $N_s = 1$ , since there was only one cell used.
- $n_{ref} = 1.3$  was assumed because it was observed that the calculated value at reference conditions was lower than those estimated in literature (Bellia *et al*, 2014), (Katsanevakis, 2011). For this reason, only 2 equations were required. Therefore Equation 21 and Equation 22 were used to solve for  $R_s$  and  $R_{sh}$ .

To solve for the parameters, the fsolve function in the python programming software (Python, 2015) was used. This is because it was observed to converge quickly and also provided accurate results when compared to the Newton-Raphson method. The code for generating the I-V curve is attached in Appendix B.

## 2.4 Modelling results

The model was fit onto the experimental data collected at  $980 \text{ W}\cdot\text{m}^{-2}$  and  $25 \text{ }^\circ\text{C}$  cell temperature. From Figure 15, it is observed that the model provides a good fit when compared to the experimental data and so the model could then be used for other experiments to obtain the parameters that could be used to analyse the behaviour of the PV cell.

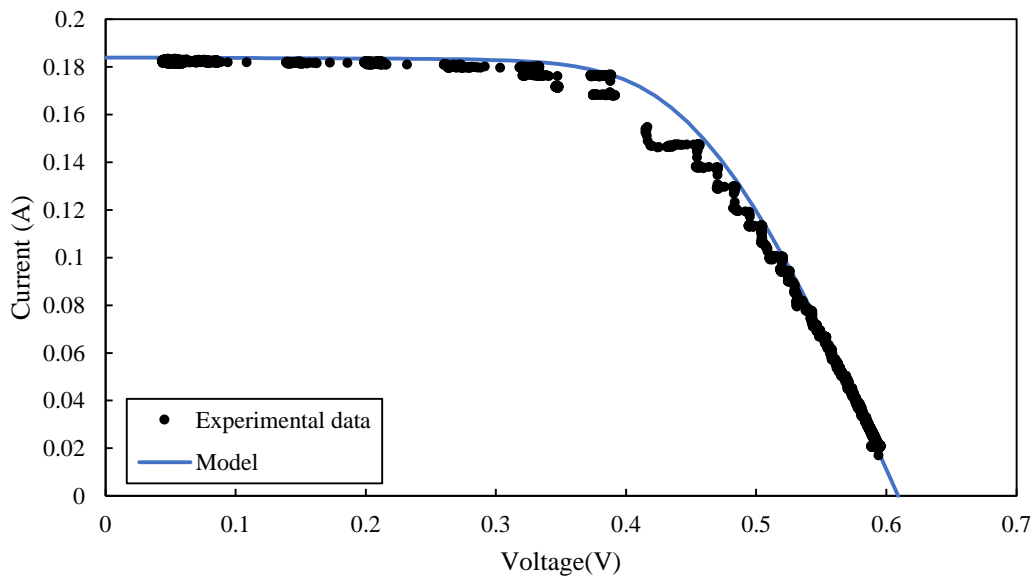


Figure 15: Schematic comparing experimental graph to the model used.

## 3. Experimental Method

### 3.1 Apparatus

#### 3.1.1 Solar Concentrator

The experiments were carried out at the University of Pretoria, South Africa's pilot scale solar concentrator (Latitude - 25°45' 02.5" Longitude 28°15' 36.2"). The concentrator consists of a primary mirror on a dual-axis tracking system. The mirror reflects incoming radiation towards a secondary mirror which subsequently redirects the light onto a circular Fresnel lens of diameter, 1 m. The circular Fresnel lens has a convex face on one side and a planar face on the other as shown on Figure 16. This results in light rays converging to a set area.

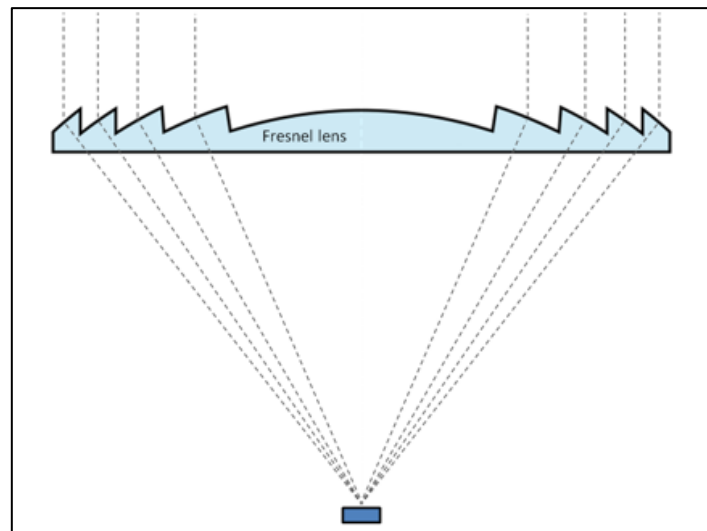


Figure 16: Schematic showing how a Fresnel lens concentrates light

#### 3.1.2 Spectral beam splitter (Optical filter)

A short pass dichroic mirror with a cut-off wavelength of 1000 nm was used to transmit wavelengths. This optical filter was selected because it provided a wavelength transmittance between 450 nm – 1000 nm at 45° which is very close to the spectral response range of polycrystalline solar cells; 300 nm – 1200 nm (Sara, Betts & Gottschalg, 2014). Figure 17 shows the transmittance and reflectance data for the optical filter provided by the supplier at 45° (Thorlabs.com, 2016). The reflectance data is also shown to confirm that the optical filter does not absorb any of the wavelengths. In addition, to confirm that the shorter wavelengths were not

transmitted, a Cary 100 UV-Visible spectrometer was used to measure the transmittance of the optical filter. This result is shown in Figure 18.

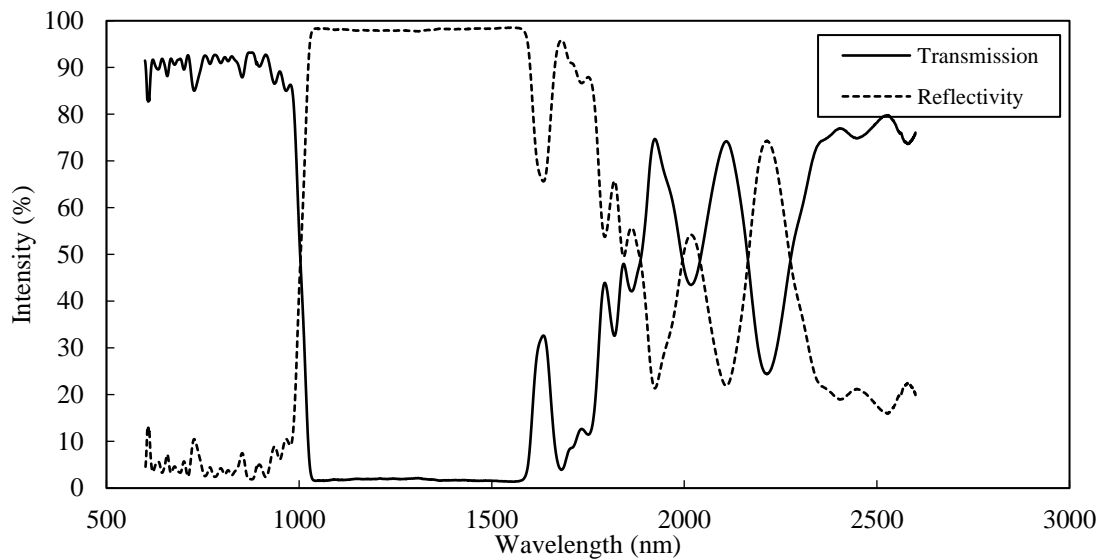


Figure 17: Transmission and reflectivity data for the spectral beam splitter

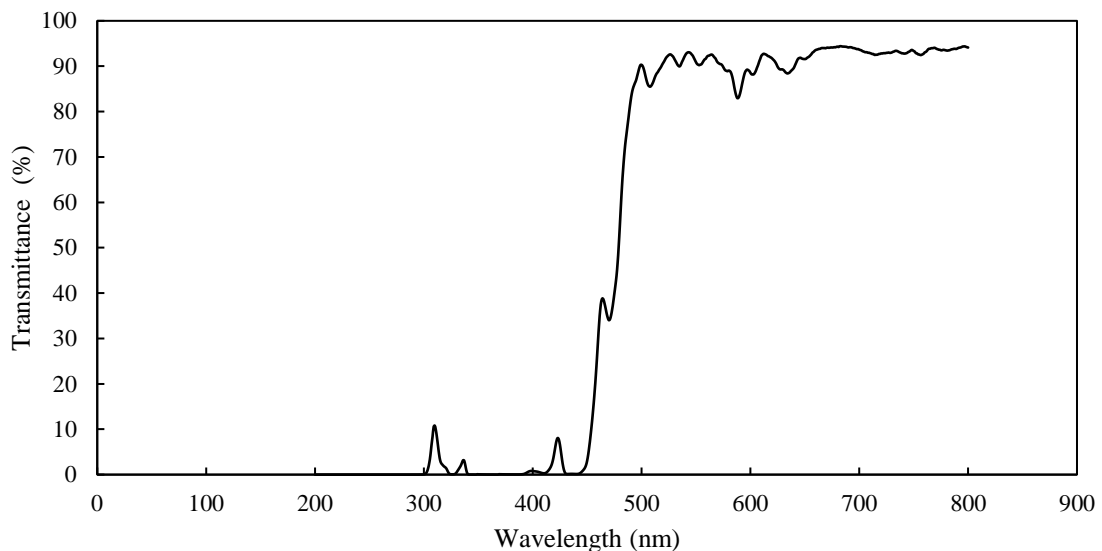


Figure 18: Transmittance measurement of the optical filter at 45°. Wavelengths greater than 450 nm are transmitted

### 3.1.3 Light intensity measurements

The experiments were done outdoors during the day between 11:00 am and 1.00 pm when the light intensity remained relatively constant. This was confirmed using the SAURAN database which provides data that has been measured by the UPR – GIZ University of Pretoria measurement station.

Additionally, an M-900 pyranometer was used to measure the Direct Normal Irradiation(DNI) that was incident to the PV cell under the lens for light intensities up to  $1000 \text{ W}\cdot\text{m}^{-2}$ . For light intensities

above  $1000 \text{ W}\cdot\text{m}^{-2}$ , the geometry method was used (Kreith, Krumdieck & Kreider, 2010: 561); the light intensity at the centre of the aperture as well as the area of the Fresnel lens that was exposed to the incident solar radiation were measured. The area where the solar cell was placed was also measured. The ratio of the two areas was used to determine the concentration ratio. The light intensity at the Fresnel lens was adjusted accordingly to determine the new light intensity. Using this method, the area could then be adjusted by changing the height of the solar cell relative to the Fresnel lens to reach the desired light intensity.

To determine the light intensity of the incident irradiance that was transmitted and reflected by the optical filter, the total area under the Direct Normal Irradiation (DNI) solar spectrum shown in Figure 19 was calculated. The ratio of the split between transmittance and reflectance was determined by calculating the area under the transmittance region based on the transmittance wavelengths from Figure 17 and Figure 18 (450 nm to 1000 nm), and subtracting it from the total area to quantify the reflectance.

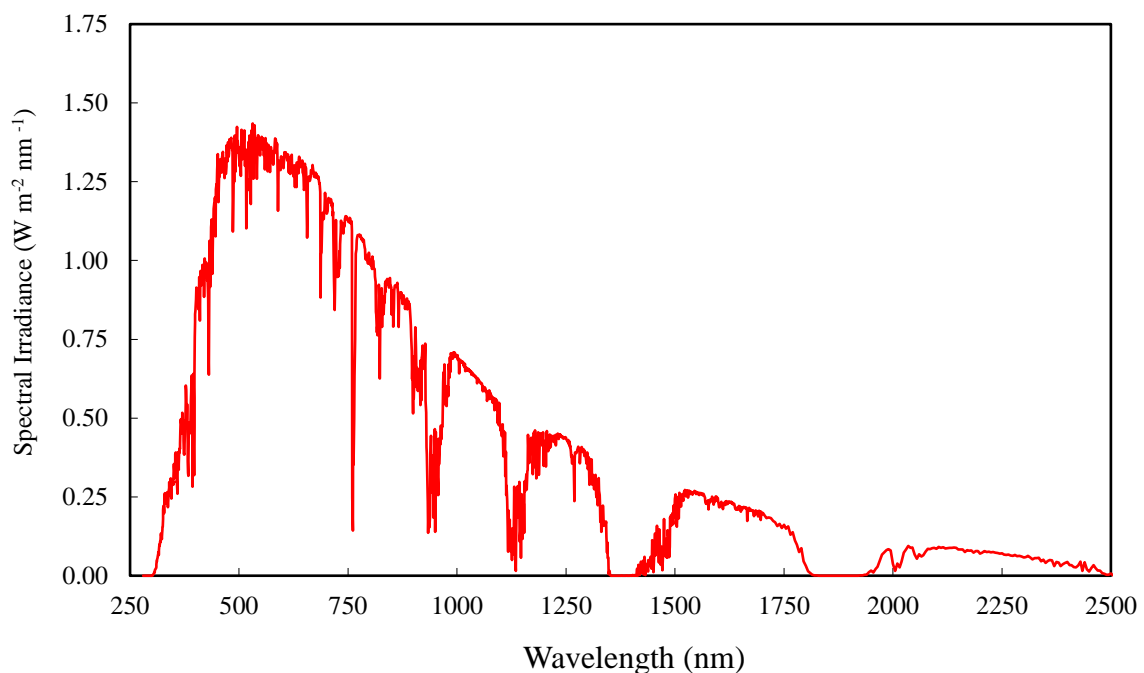


Figure 19: Spectral irradiance data (A.M 1.5D)

### 3.1.4 Generating a characteristic IV curve

A 0.5 V, 100 mA,  $53 \text{ mm} \times 18 \text{ mm} \times 2.5 \text{ mm}$  polycrystalline PV cell was placed under the Fresnel lens. The load was varied using a  $25 \Omega$ , 12.5 W, 0.71 A rheostat which was gradually adjusted at a constant rate by rotating the knob clockwise in order to generate the characteristic I-V curve. The experimental data acquisition of the current and voltage was carried out using a National Instruments (NI) DAQ module that was managed using LabVIEW software.

A k-type thermocouple was attached to the DAQ module to measure the temperature of the PV cell. To analyse the I-V curves, the single diode equation, (Equation 1) was used to fit a line to the generated IV curve. The desired parameters;  $I_{ph}$ ,  $I_o$ ,  $R_{sh}$  and  $R_s$  could then be obtained from the fitted curve.

### 3.1.5 External cooling

For experiments that required cooling, a fin was attached to the bottom of the PV cell using silicon thermal paste. A Watson Marlow 323S/D pump was used to pump water across the set-up. To prevent the cooling water from heating up during experimentation, the set-up was covered with aluminium foil. The foil was laid as flat as possible to minimise diffuse reflectance from its surface.

A schematic and a picture of the set-up used for experimentation is shown in Figure 20.

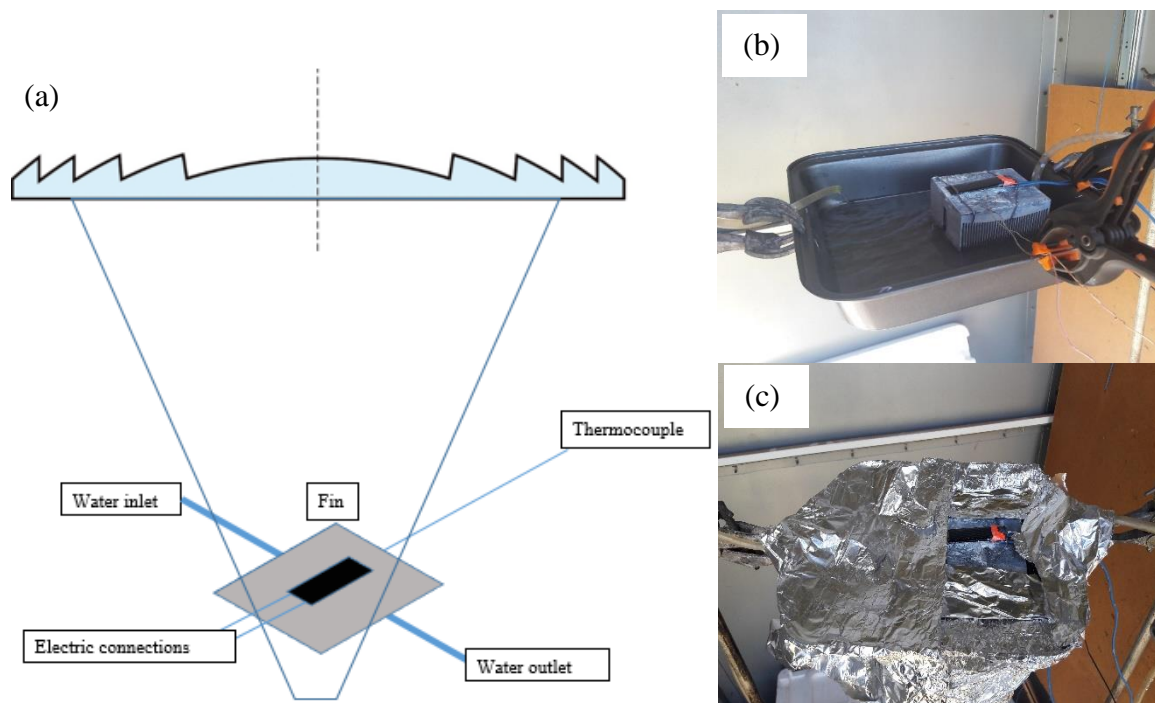


Figure 20: a) Sketch illustrating experimental set-up, b) Picture of the experimental setup, c) Picture showing the experimental set-up covered with foil to prevent heating of water.

### 3.2 Experimental design

Five experiments were carried out to obtain parameters required to characterise the PV cell. The light intensity incident on the PV cell, cell temperature, current and voltage were measured. The experiments looked at the influence of the spectral beam splitting on temperature, and on the performance of the PV cells. Additionally, experiments were carried out to determine if the

performance of the PV cell changed as a function of temperature and light intensity. The experimental procedures are described below.

### 3.2.1 Influence of optical filter on the temperature of a PV cell (same light intensity)

To determine if spectral beam splitting influenced the temperature of the PV cell, two polycrystalline PV cells were placed side by side under the Fresnel lens and operated at a constant load as can be seen in Figure 21.

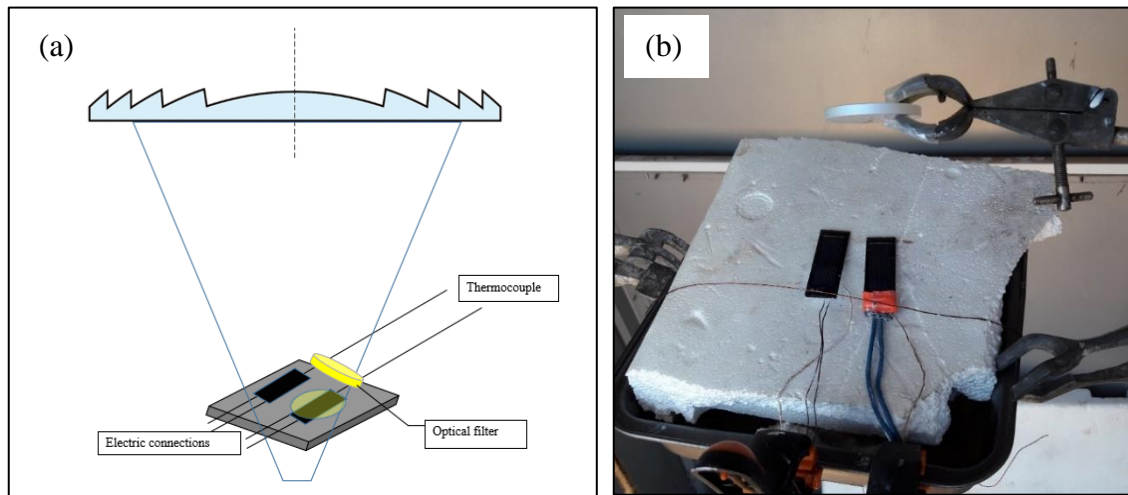


Figure 21: a) Side view sketch of the setup b) Photograph of the experimental set up

The temperature was chosen as the dependent variable with the understanding that wavelengths that do not produce a spectral response in the polycrystalline PV cell are converted to heat, which has been shown to decrease the efficiency of the PV cell (Mojiri *et al*, 2013).

Prior to experimentation, the two PV cells were tested under the same conditions ( $980 \text{ W}\cdot\text{m}^{-2}$  and  $25^\circ\text{C}$  cell temperature) to ensure that they produced the same characteristic IV-curve.

One PV cell was placed 10 cm below the optical filter and the other PV cell was left exposed to the incident irradiation. The PV cells were placed on a polystyrene block to prevent heat losses from the back surface to the surrounding. A constant load was applied to the cell by adjusting the resistor knob to the point where a maximum load was measured by the DAQ module.

To start the experiment, the supporting tray was placed at a height where the incident light intensity on the PV cell was  $980 \text{ W}\cdot\text{m}^{-2}$ . The initial cell temperature and ambient temperature were measured to confirm that the cell was operating at  $25^\circ\text{C}$ . The values used were close to concentrator standard test conditions for Direct Normal Irradiation (DNI);  $1000 \text{ W}\cdot\text{m}^{-2}$ ,  $25^\circ\text{C}$  cell temperature and an air mass (A.M) of 1.5 (Pérez-Higueras & Fernández, 2015: 118).

The setup was then left to operate for one hour and the temperature was measured at 2 minute intervals. At the point where the temperature was observed to remain unchanged with time, measurements were then taken at 5 minute intervals. The light intensity was measured after every half hour interval to ensure that there was no significant variation in light intensity and to minimise any effect of shading on the PV cells.

### **3.2.2 Quantifying the temperature change and efficiency of the PV cell for transmitted and reflected light**

To determine the effect of the transmitted and the reflected wavelengths of the solar spectrum on the performance of the PV cell, the temperature change of the cell, and the cell's efficiency were required.

As can be seen from Figure 22, the PV cells were placed perpendicular to each other. Two similar polycrystalline solar cells were encased in polycrystalline sheets to minimise heat losses from the surface of the solar cell through convection. The optical filter was used to split the spectrum with the bottom panel receiving transmitted light (450 nm – 1000 nm), while the perpendicular panel received wavelengths outside this range of the solar spectrum. The polystyrene case at the back of the perpendicular cell was covered using aluminium foil to ensure that the cell's increased temperature was solely due to the reflected light from the filter.

The experiment was carried out isothermally; the I-V curve was obtained as soon as the experiment began. The temperature of the cell was measured throughout experimentation to confirm that the temperature of the cell remained unchanged.

Thereafter, the setup was left for one hour at constant load. The temperatures of both cells were collected at 2 minute intervals until the temperatures of the cells were observed to remain unchanged. Thereafter the temperatures were collected at 5 minute intervals.



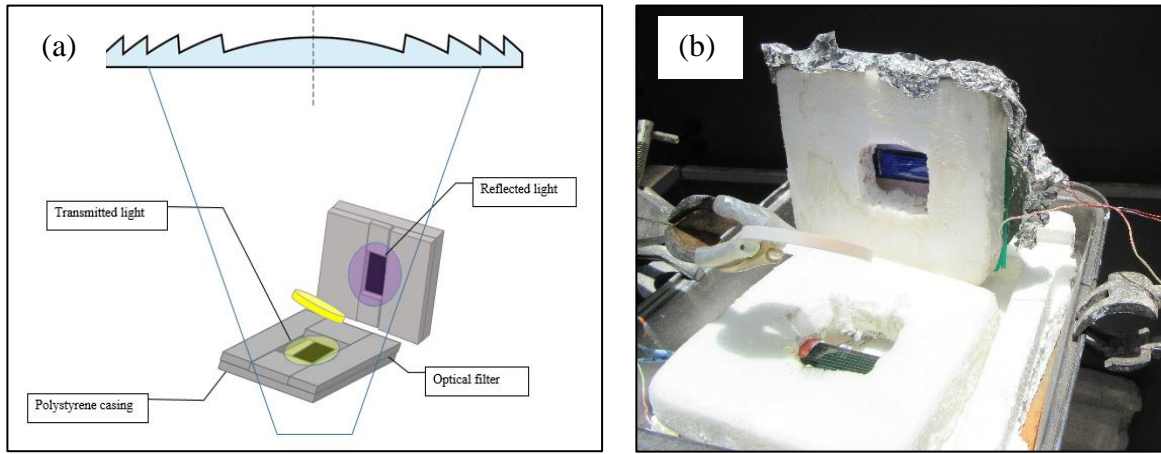


Figure 22: PV cells under illumination: a) schematic of setup, b) photograph of setup

### 3.2.3 Influence of optical filter on the performance of a PV cell at constant temperature

The reason for applying spectral beam splitting to PV cells, is to ensure that wavelengths incident on the panel that do not produce a spectral response and instead decrease efficiency of the solar cell, are filtered off. This experiment was carried out to determine if the efficiency of the PV cell was affected by filtering off the wavelengths outside the PV cell's spectral response range.

The light intensity and the cell temperature for the experimental set-up were left unchanged for the full duration of the experiment to ensure that any change observed was solely due to spectral beam splitting. The maximum power of the cell was the dependent variable because it provided an indication of highest amount of electricity that can be obtained from the incident solar radiation. The efficiency of the PV cell was then calculated using Equation 5.

Two separate experiments were carried out using the set-up shown in Figure 23. Before any measurements could be taken, the pump was initiated at 100 rpm; the flow rate which resulted allowed the cell temperature to remain between  $25^{\circ}\text{C} - 27^{\circ}\text{C}$ . The set-up was left to run for 5 minutes to ensure that the cell was at a constant temperature. The light intensity was then measured using the pyranometer. The characteristic I-V curve was generated by varying the load across the resistor at a constant rate from 0 V to the open circuit voltage value. The temperature of the PV cell was monitored to ensure it remained unchanged while data was collected. Five readings were taken for each experiment to ensure repeatability.

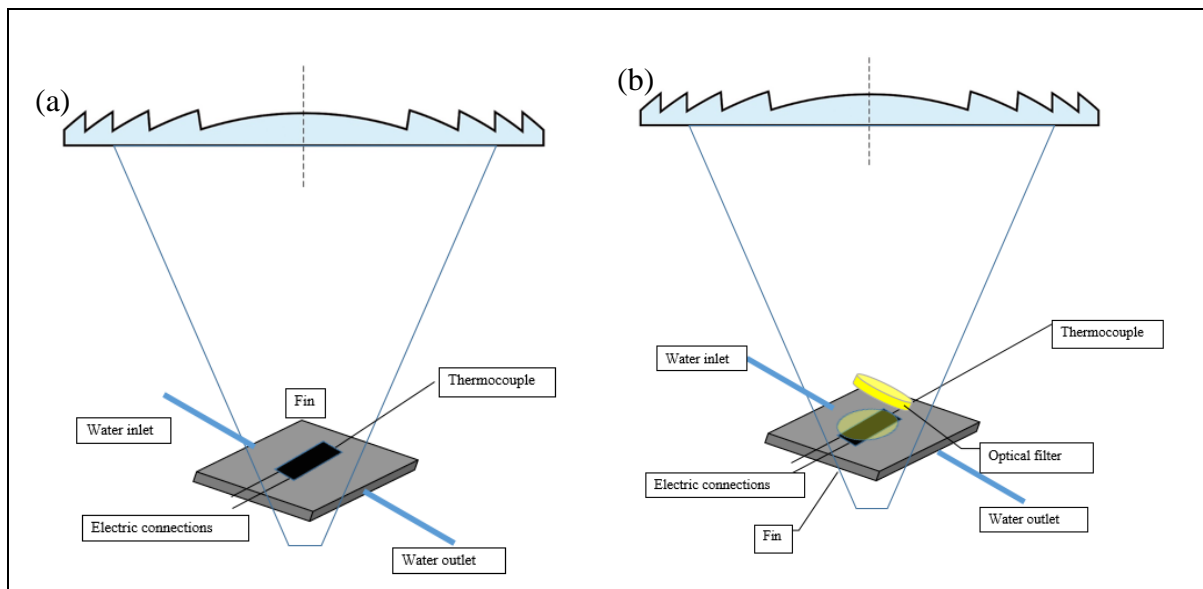


Figure 23: Diagram of the experimental set-up a) No filter, b) Filter

### 3.2.4 Influence of optical filter on the performance of a PV cell with varying temperature

The efficiency of PV cells decreases with increased cell temperature (Green, 1982). A PV cell generates electricity only when exposed to specific wavelengths. Wavelengths that are outside this range are converted to heat (Mojiri *et al*, 2013). Therefore, this experiment was used to determine how splitting the solar spectrum would affect efficiency of the PV cell if the temperature of the cell increases.

The maximum power of the cell was the dependent variable because it provided an indication of how much of the incident radiation was converted into electricity. The I-V curve was also studied to determine how the FF,  $V_{oc}$  and  $I_{sc}$  changed to influence the maximum power of the PV cell.

Two experimental setups were used; one with the filter and another without a filter using a setup similar to Figure 23. For each setup, a polycrystalline PV cell was placed on a polystyrene sheet to prevent heat losses from the back surface of the cell. The experimental setups were initially cooled to operate between  $25^{\circ}\text{C}$  -  $27^{\circ}\text{C}$ . The initial temperature of the cell was measured and the I-V curve was obtained at the beginning of the experiment. Thereafter, the external cooling was removed and the I-V curve was generated at 5 minute intervals for one hour. Finally, the I-V curves were compared and the efficiency of the cells determined.

### 3.2.5 Influence of light intensity on the performance of a PV cell

At isothermal conditions, increasing the light intensity increases the efficiency of the polycrystalline cells. This can be attributed to the increase in the short circuit current and the increase in open circuit voltage. However, the short circuit current is more sensitive to light intensity than the open circuit voltage (Chegaar *et al*, 2013). At high light intensities however, the parasitic resistances cause the

efficiency to decrease. The objective of this experiment was to determine if the optical filter affected the change in efficiency of the PV cell as the light intensity increased.

A similar experimental setup to Figure 23 and the experimental procedure as described in section 3.2.3 was used. I-V curves were obtained between  $580 \text{ W}\cdot\text{m}^{-2}$  and  $1380 \text{ W}\cdot\text{m}^{-2}$ . The experimental setup was attached to two retort stands which could be adjusted by unwinding the clamping screw from the stand and positioning the setup at the desired height. The setup is shown in Figure 24.

The initial light intensity was measured and the I-V graph was generated 3 – 5 times. Thereafter the setup was lowered to increase the light intensity. The experiment was carried out for the setup with the optical filter and repeated for the setup in the absence of the optical filter.

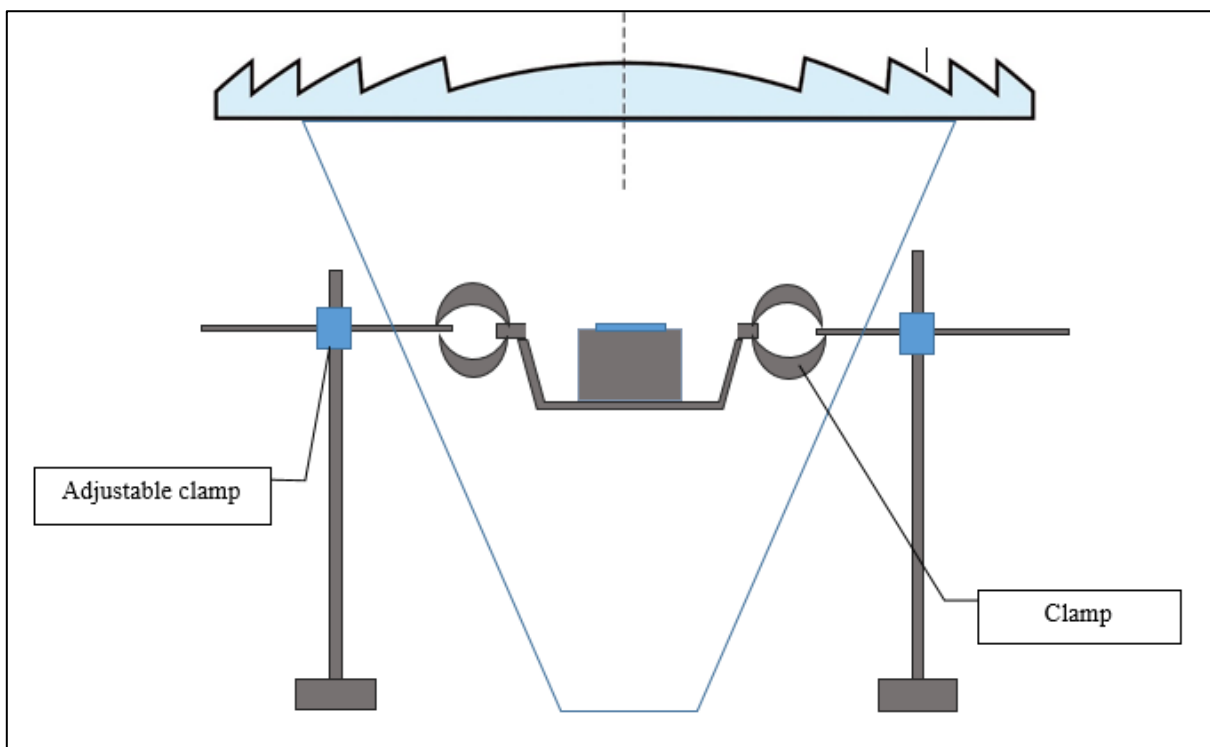


Figure 24: Schematic of the experimental setup used to adjust for light intensity.

## 4. Results and Discussion

The results presented in this chapter look at the influence of light intensity and temperature on the performance of a polycrystalline silicon PV cell that is exposed to wavelengths between 450 nm – 1000 nm. In order to make this observation, the PV cell under the optical filter is compared to a PV cell in the absence of an optical filter. The main PV cell factors that have been looked at are the cell temperature ( $T_c$ ), cell efficiency ( $\eta$ ) and the maximum power ( $P_{max}$ ). The changes in the PV cell parameters: FF,  $I_{sc}$ ,  $V_{oc}$  and  $R_{sh}$  are observed to explain the observed change in  $\eta$  and  $P_{max}$ . These PV cell parameters are determined using the model discussed in Chapter 2.

### 4.1 Influence of the optical filter on the temperature of a PV cell (same light intensity)

This experiment compares the temperature change of the PV cell under an optical filter to that of a PV cell without a filter. Figure 25 shows the temperature of the PV cells increasing gradually for the first 10 minutes. Thereafter, the temperature remains unchanged. The temperature difference between the spectrally filtered setup and the spectrally unfiltered setup is determined to be 11 °C throughout the experiment.

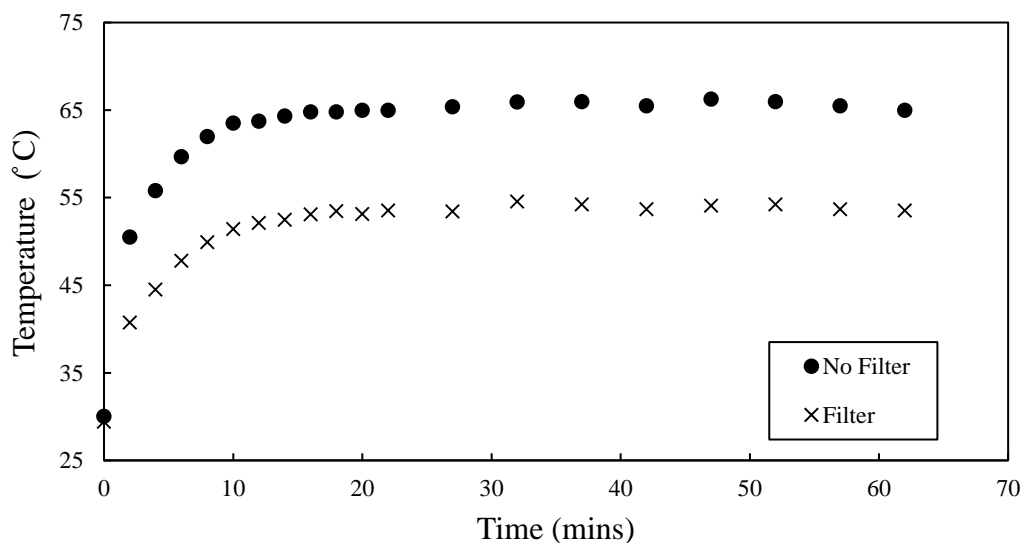


Figure 25: Temperature change of the PV cells under illumination.

Additionally, the temperature of the PV cell receiving the full solar spectrum is higher than the temperature of the PV cell that is under the filtered solar spectrum. This is in agreement with the understanding that wavelengths outside the range 450 nm – 1000 nm which are not converted into electricity, contribute to heating the cell. Therefore, it results in a higher PV cell temperature

compared to the setup that is exposed to wavelengths within the specified range (Imenes & Mills, 2004).

#### 4.2 Quantifying the temperature change of the PV cell for transmitted and reflected light

It has already been established that the wavelengths of the solar spectrum influence the temperature of PV cells. Figure 26 shows the normalised temperature change for the PV cells that were exposed to transmitted incident light (450 nm – 1000 nm) and the reflected incident light of the solar spectrum. The temperatures have been normalised to the incident radiation to make the data from the transmitted and reflected spectrum comparable. A higher normalised temperature change is observed for the PV cell under the reflected light. This is because a significant portion of the reflected wavelengths do not match the energy band gap of the polycrystalline PV cell. The reflected wavelengths are UV and Near IR. Although UV light is able to produce electron hole pairs, it has excessive energy which results in thermal energy being released from the PV cell. Near IR does not have enough energy to induce electron hole pair formation and is also dissipated usually as heat.

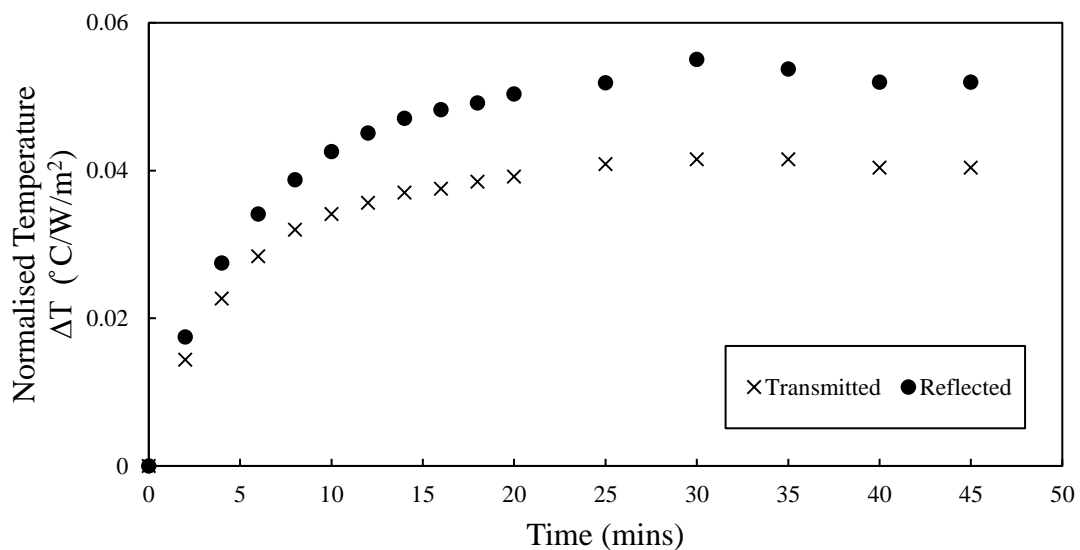


Figure 26: Normalised temperatures for PV cells exposed to transmitted and reflected light

#### 4.3 Influence of spectral beam splitting on the performance of a PV cell at isothermal conditions

Figure 27 contrasts the characteristic I-V curve and the P-V curve for the PV cell under a spectrally split spectrum with an unfiltered spectrum. It can be seen that spectral beam splitting reduces the maximum power of the PV cell. The power is calculated to decrease by 18.5 %. Additionally, the decrease in power is observed to be mainly affected by the decrease in the short circuit current ( $I_{sc}$ ).

This is because the wavelengths in the range of 300 nm – 450 nm and 1000 nm - 1200 nm which are known to produce a spectral response from polycrystalline PV cells (Sara *et al*, 2014), are not transmitted through the filter to the PV cell. A slight decrease in the open circuit voltage ( $V_{oc}$ ) is also observed, according to Equation 10, decreasing the light intensity, decreases the open circuit voltage of PV cell.

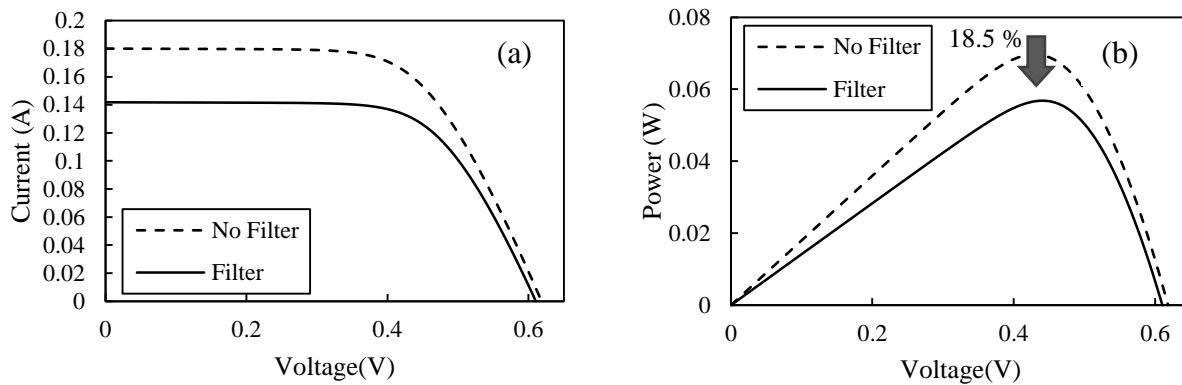


Figure 27: a) Characteristic I-V curve for the PV cell at 25 °C, b) Power-Voltage curve for the PV cell at 25 °C

Table 2 shows the parameters of the irradiance that is incident to the PV cell while Table 3 shows the PV cell parameters extracted from the model. From Table 3, it is observed that the efficiency of the PV cell increases by 2.1 %. This is because of the improved matching of the incident radiation to the spectral response of the PV cell; the PV cell is exposed to wavelengths that can produce a spectral response.

Table 2: Comparison between filtered and unfiltered PV cells

	Filter	No Filter	Unit
Light intensity	980	980	$W \cdot m^{-2}$
Light intensity (Incident on PV cell)	622	980	$W \cdot m^{-2}$
Cell area	0.000954	0.000954	$m^2$
Power in	0.594	0.935	W

Table 3: Numerical results for PV cell parameters

Setup	$V_{oc}$ (V)	$I_{sc}$ (A)	$R_s$ ( $\Omega$ )	$R_{sh}$ ( $\Omega$ )	Standard deviation (%)	Fill Factor (FF)	Efficiency (%)
Filter	0.61	0.14	0.586	728	1	0.67	9.56
No Filter	0.62	0.18	0.675	568	1	0.63	7.45

Additionally, we see from Table 3, that the increase in efficiency is due to the increase in the fill factor which is influenced by the decrease in the series resistance and the increase in the shunt resistance which both increase the fill factor as is confirmed by Figure 6. The model assumed a constant value for the series resistance. The reason for the observed change in the  $R_s$  value, is that any slight adjustment to the  $V_{oc}$  affected this value. The  $R_s$  represents the slope at  $V_{oc}$ . The  $V_{oc}$  at reference conditions in the model had to be adjusted to increase the accuracy of the fit. However, the changes were within the standard deviation.

#### 4.4 Influence of optical filter on the performance of a PV cell with varying temperature

To determine the influence of temperature on the performance of polycrystalline silicon solar cells, the I-V curves for the PV cell under the transmitted, reflected and the full solar spectrum were generated at the beginning of the experiment ( $980 \text{ W}\cdot\text{m}^{-2}$  and  $25^\circ\text{C}$  cell temperature) and after 45 minutes with no external cooling. The changes in the PV cell parameters could then be determined as illustrated in Figure 28.

From Figure 28, the open circuit voltage is observed to decrease with increased temperature, for all experimental setups. However, no change is observed in the short circuit current for the filtered, while the short circuit current is observed to increase slightly for the unfiltered setup.

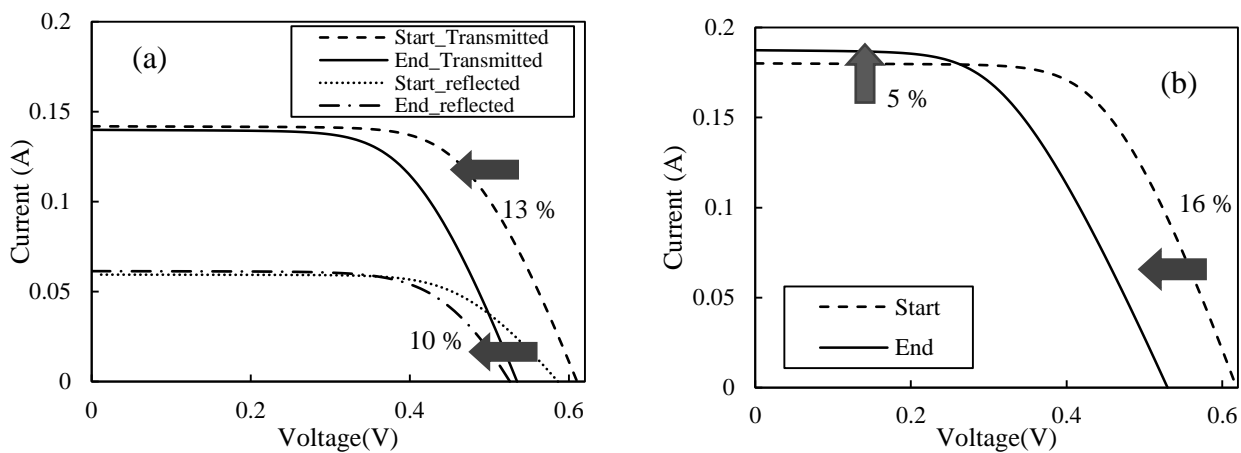


Figure 28: I-V curves showing change of performance of PV cells as a function of temperature. a) Filtered setup (transmitted and reflected spectrum), b) Unfiltered setup (full spectrum)

The change in the short circuit current as a function of temperature depends mainly on the change in the bandgap. The bandgap becomes smaller as temperature increases (Green, 1982: 91). For polycrystalline silicon PV cells, this means that the longer wavelengths are able produce electricity resulting in an increase in the short circuit current. The filtered experimental setup was not exposed to the full solar spectrum and so the wavelengths outside the range  $450 \text{ nm} - 1000 \text{ nm}$ , which can

be converted to electricity, are not available. Therefore, the increase in short circuit current for the unfiltered setup would be because of the exposure of the PV cell to the full solar spectrum. The standard deviation of 1 % at the end of the experiment (Table 5), allows for comparison of these results as a function of temperature.

However, the open circuit voltage is observed to significantly decrease for both filtered and the unfiltered setup at a higher temperature. It is known that the open circuit voltage decreases with increased temperature (Green, 1982: 92). We see from Figure 28, for the setup with no filter, there is a 16 % decrease in the open circuit voltage, while for the setup with the filter, the open circuit voltage decreases by 13 %. Since the unfiltered setup was at a higher temperature than the filtered setup, it is expected to have a lower open circuit voltage. However, the standard deviation of 3 % (Table 4) at the end for the unfiltered setup means that a conclusive result cannot be reached for the effect of spectral beam splitting on the open circuit voltage as a function of temperature.

Figure 29 shows the P-V graphs measured for the filtered and unfiltered PV cell experimental setup at the start of the experiment ( $980 \text{ W}\cdot\text{m}^{-2}$  and  $25^\circ\text{C}$  cell temperature) and after one hour. The maximum power is observed to decrease for both experimental setups. However, there is a much larger decrease in the maximum power for the unfiltered setup compared to the filtered setup. This effect is attributed to the combined effect of the open circuit voltage, the short circuit current and the fill factor. This can be seen from Equation 6.

The unfiltered setup is at a higher temperature than the filtered setup which means it will have a lower open circuit voltage and a higher short circuit current. Moreover, the fill factor decreases as temperature increases (Chander *et al*, 2015) and so this result is expected. It can then be seen from Equation 5 and Equation 6 that the maximum power will decrease as the fill factor decreases.

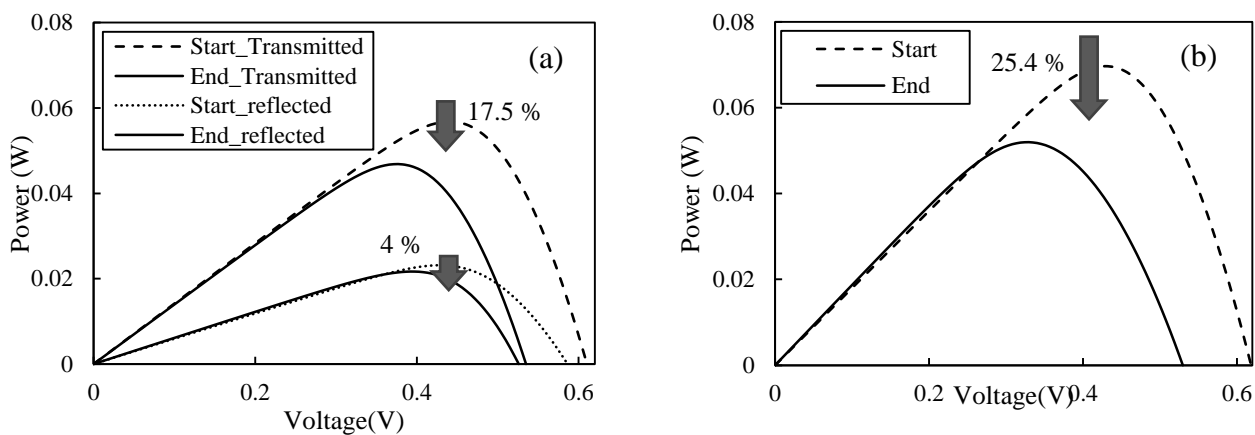


Figure 29: a) P-V curve for a) filter – transmitted and reflected spectrum, b) Power-Voltage curve (no filter)



Additionally, it is important to note that the fill factor is influenced by the resistance of the PV cell, and so changes in parasitic resistances; series resistance ( $R_s$ ) and shunt resistance ( $R_{sh}$ ), will affect the cell's operating point (Green, 1982: 96).

To confirm if there were any changes in the parasitic resistances which could have influenced the fill factor,  $R_{sh}$  values for the PV experimental setups were determined from the model. Table 4 and Table 5 show the change in  $R_s$  and  $R_{sh}$  values. The  $R_{sh}$  should decrease with increased cell temperature. This should reduce the fill factor. This is confirmed from the  $R_{sh}$  values in Table 4. The increase in the  $R_s$  value (Table 4) is large because of the standard deviation, which affects  $V_{oc}$  and therefore  $R_s$ .

For the filtered setup (Table 5) we see a small change in the  $R_s$  which is expected because this value should stay constant based on the modelling assumption. The  $R_{sh}$  value on the other hand decreases as is expected.

Table 4: Illustration of the drop in efficiency of the PV cell under the transmitted and reflected light

Setup	$T_c$ (°C)	$V_{oc}$ (V)	$I_{sc}$ (A)	$R_s$ ( $\Omega$ )	$R_{sh}$ ( $\Omega$ )	Standard deviation (%)	Fill Factor (FF)	Efficiency (%)
Transmitted spectrum								
Start_transmitted	25	0.61	0.14	0.6755	568	1	0.66	9.56
End_transmitted	52	0.53	0.14	0.8724	290	3	0.63	7.89
Difference								1.67
Reflected spectrum								
Start_reflected	25	0.59	0.06	-	-	2	0.66	6.77
End_reflected	51	0.53	0.06	-	-	3	0.67	6.34
Difference								0.43

Table 5: Drop in efficiency of the PV cell in the absence of the optical filter

Setup	T <sub>c</sub> (°C)	V <sub>oc</sub> (V)	I <sub>sc</sub> (A)	R <sub>s</sub> (Ω)	R <sub>sh</sub> (Ω)	Standard deviation (%)	Fill Factor (FF)	Efficiency (%)
Start	25	0.62	0.18	0.586	758	1	0.63	7.45
End	54	0.52	0.19	0.579	466	1	0.51	5.56
Difference								1.89

It was observed that the presence of the filter does not significantly influence the magnitude by which the efficiency of the PV cell drops. This can be seen from Table 4 and Table 5 where the drop in the efficiency for the unfiltered setup is slightly higher compared to the filtered setup. However, the efficiency difference between the filtered and unfiltered experimental setup at the end of the experiments is 2.33 % which means that although the efficiency drops, spectral beam splitting does not influence the difference in efficiency of the PV cell at the reference condition.

Furthermore, it is observed that the temperature difference between the filtered and unfiltered setup is 2 °C. The small temperature difference is because the resistor was continuously adjusted at time intervals and so the experiment was not operating at a constant load. This means that the amount of energy converted into heat during experimentation is not consistent.

Figure 28(a) shows how the I-V curve for the PV cell changed as a function of temperature when it was exposed to the reflected wavelengths outside the range 450 nm – 1000 nm of the solar spectrum. The model did not provide a good fit for the reflected spectrum and so the parameters were adjusted to fit the curve and only parameters that could be read off the I-V curve were tabulated.

From the change in the I-V curve, we can see a drop in the open circuit voltage. This decrease in the open circuit voltage can also be explained by the dependence of V<sub>oc</sub> on the temperature. The short circuit current remains unchanged. However, from Table 4, we can see that the change in the cell parameters for the PV cell under the reflected spectrum is not very significant; the fill factor only changes at the second decimal place. From Figure 29(a), we observe a small decrease in power of 4% which is mainly because of the decrease in in the open circuit voltage.

The small variation in the fill factor for the PV cell under the reflected spectrum in Table 4, gives an indication that the parasitic resistances do not significantly affect the efficiency. It means that the main reason for the decrease in efficiency is the decrease in the open circuit voltage.

Moreover, the temperature of the cells; under the reflected and transmitted spectrum, was the same because the light intensity on the reflected spectrum was lower than that which was incident on the transmitted spectrum. Additionally, the experiment was also not carried out at constant load, and so you would expect a different heating rate. However, we have already shown in Chapter 3.2.2 that the normalised temperature change is higher for the PV cell under the reflected spectrum compared to the transmitted spectrum.

#### 4.5 Response of PV cells to transmitted and reflected wavelength at isothermal conditions

This experiment was carried out to compare efficiencies for the different solar spectra and also to determine if the sum of power for the PV cell under the transmitted and reflected spectrum equals that of the PV cell exposed to the full spectrum.

A portion of the wavelengths, that were reflected by the optical filter were within the spectral range for a polycrystalline silicon PV cell and therefore should produce electricity. Figure 30 shows the characteristic I-V curve for the PV cell under the full spectrum, transmitted and reflected wavelengths of the solar spectrum at 25 °C. The observed short circuit current for the reflected spectrum confirms that the optical filter reflects a portion of the solar spectrum.

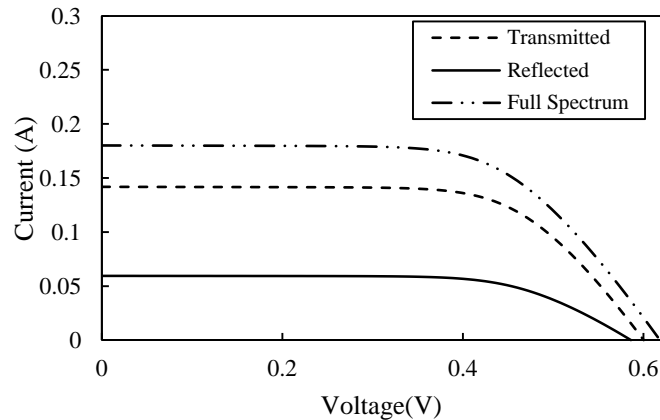


Figure 30: I-V curves for PV cells exposed to the transmitted spectrum (450 nm – 1000 nm) and reflected part of the solar spectrum

The efficiency of the cell exposed to the reflected spectrum was found to be 6.77 %, an efficiency lower than for the transmitted wavelengths (9.54 %) as can be seen in Table 6. This means that less of the photons that were incident on the reflected PV cell were converted into electricity. Additionally, adding the maximum powers for the PV cells under the transmitted and reflected spectrum results in a total of 0.08 W. We would expect the sum of these two factors to equal that

full spectrum which was determined to be 0.07 W. This difference is mainly due to the standard deviation.

Table 6: PV cell parameters and cell performance indicators

Spectrum	Light intensity ( $\text{W}\cdot\text{m}^{-2}$ )	$T_c$ ( $^{\circ}\text{C}$ )	$V_{oc}$ (V)	$I_{sc}$ (A)	Standard deviation (%)	Efficiency (%)	$P_{max}$ (W)
Full spectrum	980	25	0.62	0.18	1	7.45	0.070
Transmitted	622	25	0.60	0.14	6	9.54	0.057
Reflected	358	25	0.59	0.06	11	6.77	0.023

#### 4.6 Influence of light intensity on the performance of a PV cell under the full solar spectrum

These results are presented to determine which PV cell parameters influence the PV cell's performance under the full solar spectrum. This will make it possible to determine any differences when they are compared to PV cell under the filtered solar spectrum. It has been discussed that the power of a PV cell increases with light intensity. This has been confirmed in Figure 31. This increase is attributed to the increase in the number of photons incident to the PV cell which increase the short circuit current and the open circuit voltage. The calculation of the standard deviation and the standard error of the mean showed a very small variation. Therefore, error bars were not plotted the graph. The light intensity at  $780 \text{ W}\cdot\text{m}^{-2}$  is the anomalous result as can be seen from the maximum power value at the same light intensity in Figure 31.

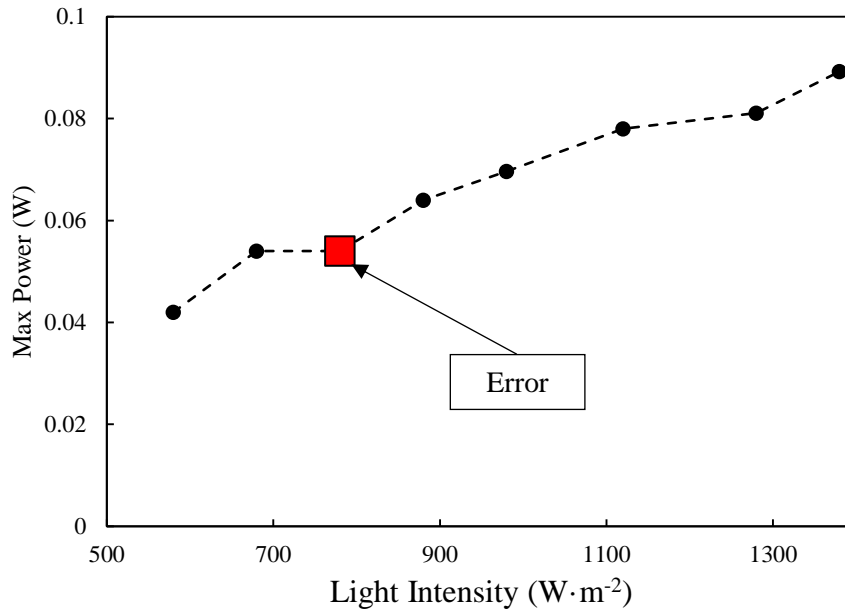


Figure 31: Change in power as a function of light intensity

It is important to note that at low voltages, the effective resistance of the PV cell is high, therefore the effect of a resistances in parallel (shunt resistances) is also high. Since the effective resistance is higher, the current will leak through these alternative paths of least resistance.

Figure 8 shows expected trend in efficiency of polycrystalline silicon PV cells with increased light intensity at low voltages. Results from the experiment carried out under the Fresnel lens in Figure 32 show an initial increase in efficiency between  $580 W \cdot m^{-2}$  and  $680 W \cdot m^{-2}$ . Thereafter, the efficiency is observed to decrease. However, the overall change in efficiency is not very significant over the flux range where the experiments were carried out.

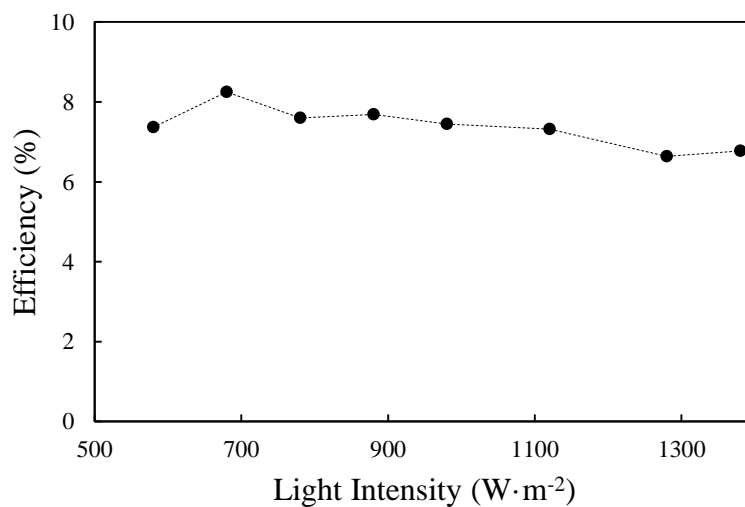


Figure 32: Illustration of the change in efficiency of a polycrystalline PV cell as a function of light intensity.

To be able to explain this behaviour the  $V_{oc}$ ,  $I_{sc}$ ,  $R_{sh}$ , and FF were all plotted as a function of light intensity. Figure 33 shows the results from the experiment. It can be seen from Figure 33(a), that the  $V_{oc}$  increases with light intensity although the increase is very small. The open circuit is expected to increase slightly but exponentially (Cuce *et al*, 2013). Similarly, the short circuit current increases as the light intensity increases as depicted in Figure 33(a). The short circuit increases linearly with light intensity which is expected (Chegaar *et al*, 2013). The model ignores the effect of  $R_s$  on the I-V curve as a function of light intensity. This means that its value should remain unchanged and so this parameter was not investigated.

Nevertheless, the fill factor is observed to decrease with light intensity as can be seen on Figure 33(a). Moreover, it is observed from Figure 33(b), that the shunt resistance decreases with light intensity. Since the fill factor is influenced by the shunt resistance and the series resistance, it can be concluded that the decrease in the fill factor is due to the decrease in the shunt resistance.

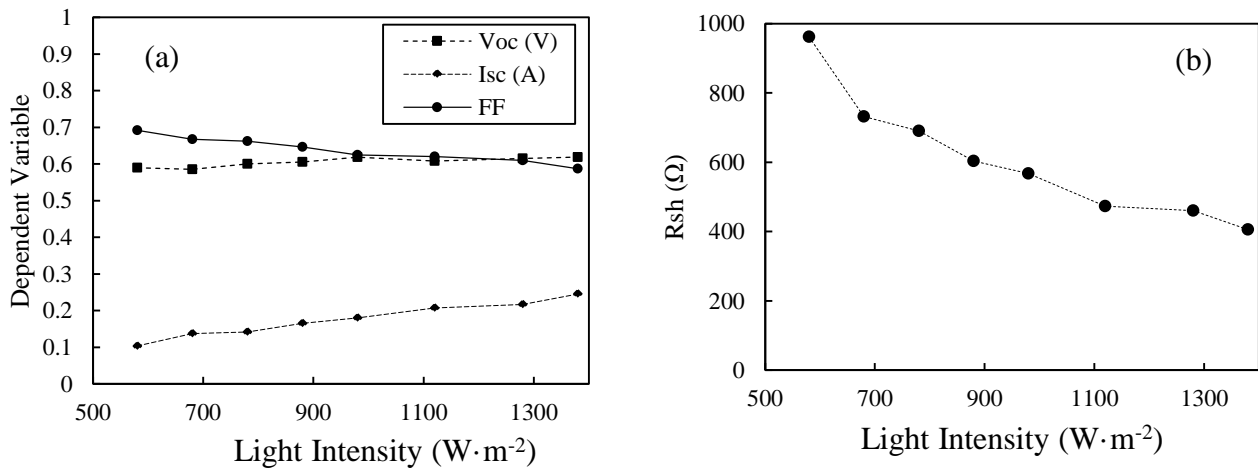


Figure 33: Influence of light intensity on: (a)  $V_{oc}$ ,  $I_{sc}$  & FF, (b)  $R_{sh}$

Using our knowledge from Equation 6 on the influence of the fill factor on the efficiency, we are able to explain the reason for the initial increase followed by a decrease in efficiency. Firstly, we note from Figure 33(a) that the open circuit voltage and the short circuit current increase with light intensity.

Between  $580 W \cdot m^{-2} - 780 W \cdot m^{-2}$ , the efficiency is observed to increase slightly. This is because the shunt resistance is high and as a result, the fill factor is also high. This means that there is less energy lost through leakages in the PV cell. However, as the light intensity continues to increase, the shunt resistance decreases which reduces the fill factor resulting in a decrease in the efficiency.

The comparison between the power and efficiency is counter intuitive; the power is observed to increase while the efficiency is observed to decrease with increased light intensity. To understand

why this is so, it is important to understand the influence of the shunt resistance. Increasing the light intensity increases the number of photons incident to the PV cell and therefore more photons are available to be converted into electricity. However, increasing the light intensity also decreases the shunt resistance and so some of the current is lost through defects within the PV cells. The shunt resistance decreases while the short circuit current increases as is seen in Figure 33(a) and Figure 33(b). Therefore, more photocurrent is available for the cell, but less of it goes into producing electricity.

#### 4.7 Influence of light intensity on the performance of a PV cell under the filtered spectrum

The purpose of this experiment was to determine if the presence of the optical filter influenced the change in the efficiency of the PV cell as the light intensity was increased. From Figure 34, it is clear that there is an initial increase in efficiency between  $580 \text{ W}\cdot\text{m}^{-2}$  to  $680 \text{ W}\cdot\text{m}^{-2}$ . Thereafter the efficiency begins to decrease. A similar trend in efficiency is observed for the filtered and unfiltered setups. However, efficiency for the filtered setup is higher than the unfiltered setup.

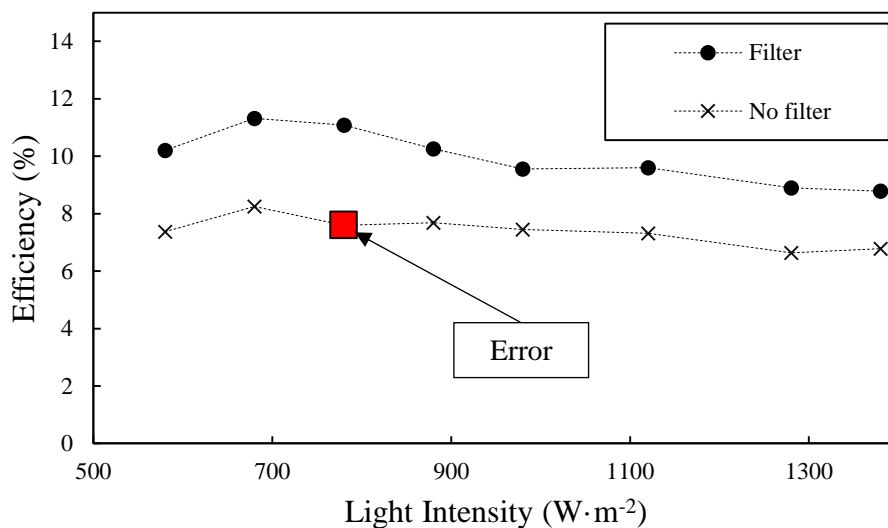


Figure 34: Comparison between PV cell with and without the filter at different light intensities

The change in the  $V_{oc}$ ,  $I_{sc}$ ,  $R_{sh}$  and FF for the PV cell under the filter were compared to the experiments carried out in the absence of the optical filter. The results are shown in Figure 35. Similarly, the small variation in the standard deviation and the standard error of the mean meant that error bars did not need to be shown on the graphs for  $V_{oc}$ ,  $I_{sc}$  and  $P_{max}$ .

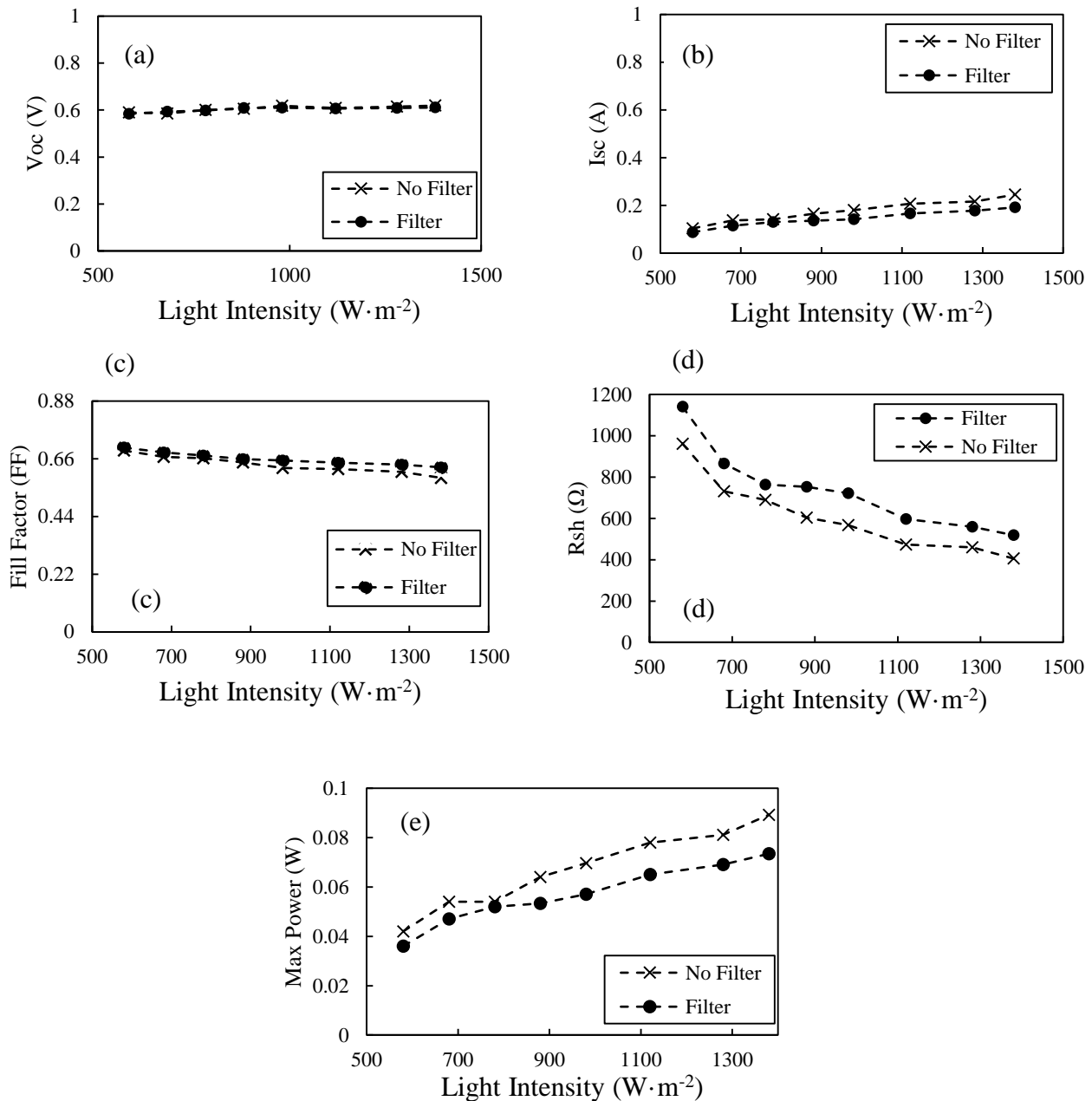


Figure 35: Comparison of PV cell parameters; (a)  $V_{oc}$ , (b)  $I_{sc}$ , (c) FF, (d) Max power and (e)  $R_{sh}$

From Figure 35(a), we can see no difference in  $V_{oc}$  between the filtered and unfiltered experimental setup. This is because  $V_{oc}$  depends significantly on the temperature which was the same for each light intensity. There is an observed increase in the short circuit current and the maximum power. This can be explained by the increase in the number of photons incident on the PV cell. Additionally, we expect the unfiltered setup to have higher values for  $I_{sc}$  (Figure 35(b)) and maximum power (Figure 35(e)) because it is exposed to the full solar spectrum that provides a wider range of wavelengths and therefore, photons with enough energy to produce electricity.



The fill factor (Figure 35(c)) is also observed to decrease with light intensity which can also be attributed to the decrease in the shunt resistance (Figure 35(d)). Furthermore, it was also observed from Figure 35 that the difference between the values for the filtered and the unfiltered setup for the FF,  $V_{oc}$  and  $I_{sc}$  increased with light intensity. Additionally, we can see from Figure 36 that the difference in efficiency between the filtered and unfiltered setup is initially high after which it is observed to decrease after  $780 \text{ W}\cdot\text{m}^{-2}$ . The large efficiency difference at  $780 \text{ W}\cdot\text{m}^{-2}$  is because there was an error in the measurement of the I-V curve at this point as is seen on Figure 31 and Figure 34.

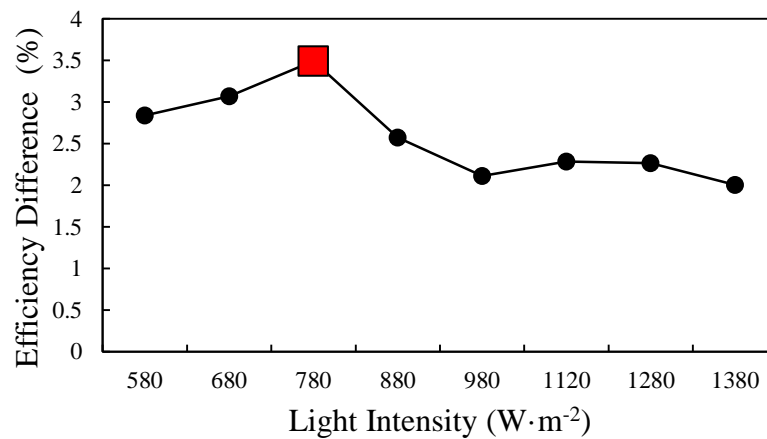


Figure 36: Efficiency difference between filtered and unfiltered experimental setups as a function of light intensity.

Explaining the reason for this decrease in efficiency difference goes beyond the scope of this research project. Further research into the interaction of wavelengths and light intensity with the bandgap of the PV cell at isothermal conditions is required to explain this trend.

## 5. Conclusions

An investigation was carried out to determine the influence of spectral beam splitting on the performance and temperature of a polycrystalline PV cell under concentrated light which was achieved using a Fresnel lens. The indicators of PV cell performance were the cell temperature ( $T_c$ ), cell efficiency ( $\eta$ ) and the maximum power ( $P_{max}$ ) of the PV cell. Spectral beam splitting was achieved using a short pass dichroic optical filter with a transmittance wavelength between 450 nm – 1000 nm. A mathematical model was used to determine the parameters  $FF$ ,  $R_{sh}$ ,  $V_{oc}$  and  $I_{sc}$  which influenced the performance of PV cells. The reference condition used was  $980 \text{ W}\cdot\text{m}^{-2}$  and a cell temperature of  $25^\circ\text{C}$ .

To determine the influence of spectral beam splitting on PV cell temperature, a comparative experiment was carried out to determine how the PV cell temperature changed when exposed to the filtered spectrum, when compared to the full spectrum. It was found that after one hour, the PV cell exposed to the full spectrum was  $11^\circ\text{C}$  higher than the PV cell exposed to the filtered spectrum. The reason for this increase in temperature is the fact that the full spectrum has wavelengths of energy that is greater than and less than the bandgap energy. This energy is dissipated in the PV cell as heat.

To further confirm this explanation, a second experiment was carried out where the normalised temperature change of two PV cells exposed to the transmitted wavelengths (450 nm – 1000 nm) and reflected wavelengths were compared. It was found that the normalised temperature change for the reflected spectrum was higher than the transmitted spectrum. Therefore, based on these results it can be concluded that exposing a polycrystalline PV cell to the solar spectra in the range of 450 nm – 1000 nm reduces the PV cell's heating rate.

The second objective was to determine if spectral beam splitting improves the efficiency of the PV cell. To achieve this, the efficiency of the PV cell was determined at isothermal conditions and at non-isothermal conditions. At isothermal conditions, it was observed that the efficiency of PV cell under the spectrally split spectrum had an efficiency of 9.54 % compared to the PV cell under the full solar spectrum which had an efficiency 7.45 %. This confirms that spectral beam splitting improves the efficiency of the PV cell by 2.1%.

A second experiment was carried out to determine the effect of spectral beam splitting on PV cell efficiency in the absence of external cooling. The efficiency of the PV cell under filtered spectrum dropped to 7.89 % while that of the PV cell under the full spectrum dropped to

5.56 %. The efficiency difference between the filtered and unfiltered experimental setup at non-isothermal conditions was 2.33 %. We can conclude from the experiments isothermal and non-isothermal conditions, that spectral beam splitting improves the efficiency of the PV cell. Nevertheless, the efficiency difference between the PV cell under the spectrally split spectrum and the full spectrum remains unchanged as temperature changes.

The third objective was to compare the effect of light intensity on the efficiency and power of the PV cell under a spectrally split spectrum to a PV cell under the full solar spectrum. This was done by varying the height between the experimental setup and the Fresnel lens in order to obtain desired light intensities.

For the PV cell under the full solar spectrum it was observed that the efficiency increased between  $580 \text{ W}\cdot\text{m}^{-2}$  –  $680 \text{ W}\cdot\text{m}^{-2}$ . Thereafter, the efficiency decreased up to  $1480 \text{ W}\cdot\text{m}^{-2}$ . Further investigation into the PV cell parameters revealed that the decrease in efficiency of the PV cell was attributed to the fill factor which is the only parameter which decreased as light intensity. This decrease in fill factor was caused by the decrease in the shunt resistance of the PV cell. The shunt resistance had a small impact between  $580 \text{ W}\cdot\text{m}^{-2}$  –  $680 \text{ W}\cdot\text{m}^{-2}$  because its value was very high; there was less leakage of current towards the edges of the cell. Based on these results we are able to conclude that the efficiency of PV cell under the full spectrum increases initially then decreases with increased light intensity because of the effect of the shunt resistance on the fill factor.

The experiment carried out for the PV cell under the split spectrum showed a similar trend in the efficiency to that of the PV cell under the full spectrum. Additionally, an investigation into the PV cell parameters also concluded that the decrease in the shunt resistance was reason for the decreased PV cell efficiency. Furthermore, comparing the efficiency difference between the filtered and unfiltered PV cells showed a difference of approximately 3 % between  $580 \text{ W}\cdot\text{m}^{-2}$  and  $780 \text{ W}\cdot\text{m}^{-2}$ , after which the difference in efficiency continued to drop to approximately 2 %. A look into the differences in FF, P<sub>max</sub> and I<sub>sc</sub> between the filtered setup and the setup exposed to the full solar spectrum, showed an opposite result where initially the difference was small after which it continued to increase.

From these results we conclude that spectral beam splitting influences how the efficiency of a polycrystalline PV cell changes. The trend in PV efficiency for the PV cell under the split spectrum is similar to that of the PV cell under the full solar spectrum. However, the difference in efficiency with increased light intensity varies. To be able to explain this difference, an

understanding of the interaction of wavelengths on the bandgaps of PV cells at constant temperature needs to be developed.

The application of spectral beam splitting to CPV has the potential to improve the efficiency of PV cells and reduce heating of PV cells. Nevertheless, we have seen that there is a contrast between an increase in power and decrease in efficiency with increased light intensity. An optimisation between maximum power and efficiency would have to be carried out. This will make it possible to determine if it makes sense to operate the silicon PV cell with an optical filter at a higher light intensity relative to standard conditions.

## **6. Recommendations**

The purpose of this report was to study the effect of spectral beam splitting on the performance of polycrystalline silicon PV cells. The research project had limitations which if accounted for could provide holistic results. To be able to achieve this, the following recommendations have been made.

A large part of the research focused on spectral beam splitting. This meant that there was a need to understand how the solar spectrum changed as a function of light intensity. It is recommended that a spectroradiometer that spans through the full solar spectrum is used to be able to observe the change in the solar spectrum with light intensity. This will also clearly determine the solar spectrum under the filter and to account for wavelengths about 1400 nm.

Additionally, based on the observations made into the effect of light intensity on the efficiency of PV cells, it is also recommended that further research is carried out to understand the interaction between the wavelengths of the solar spectrum on the bandgap of polycrystalline PV cells at isothermal conditions.

## 7. References

- Amillo, A, Huld, T, Vourlioti, P, Müller, R & Norton, M (2015), "Application of Satellite-Based Spectrally-Resolved Solar Radiation Data to PV Performance Studies" *Energies*, 8(5), 3455.
- Arrasmith, WW (2015) *Systems Engineering and Analysis of Electro-Optical and Infrared Systems*, CRC Press.
- Bellia, H, Youcef, R & Fatima, M (2014), "A detailed modeling of photovoltaic module using MATLAB" *NRIAG Journal of Astronomy and Geophysics*, 3(1), 53-61.
- Bensalem, S & Chegaar, M (2013), "Thermal behavior of parasitic resistances of polycrystalline silicon solar cells" *Revue des Energies Renouvelables*, 16(1), 171 - 176.
- BP (2017) *BP Statistical Review of World Energy 2017*.
- Chander, S, Purohit, A, Sharma, A, Arvind, Nehra, SP & Dhaka, MS (2015), "A study on photovoltaic parameters of mono-crystalline silicon solar cell with cell temperature" *Energy Reports*, 1(Supplement C), 104-109.
- Chegaar, M, Hamzaoui, A, Namoda, A, Petit, P, Aillerie, M & Herguth, A (2013), "Effect of Illumination Intensity on Solar Cells Parameters" *Energy Procedia*, 36, 722-729.
- Chendo, MAC, Jacobson, MR & Osborn, DE (1987), "Liquid and thin-film filters for hybrid solar energy conversion systems" *Solar & Wind Technology*, 4(2), 131-138.
- Cuce, E, Cuce, PM & Bali, T (2013), "An experimental analysis of illumination intensity and temperature dependency of photovoltaic cell parameters" *Applied Energy*, 111, 374-382.
- de Blas, MA, Torres, JL, Prieto, E & García, A (2002), "Selecting a suitable model for characterizing photovoltaic devices" *Renewable Energy*, 25(3), 371-380.
- De Soto, W, Klein, SA & Beckman, WA (2006), "Improvement and validation of a model for photovoltaic array performance" *Solar Energy*, 80(1), 78-88.
- DeSandre, L, Song, D, Macleod, H, Jacobson, M & Osborn, D (1985), "Thin-Film Multilayer Filter Designs For Hybrid Solar Energy Conversion Systems" *Optical Materials Technology for Energy Efficiency and Solar Energy Conversion IV*, 155.
- El-Shaer, A, Tadros, M & Khalifa, M (2014), "Effect of Light Intensity and Temperature on Crystalline Silicon Solar Modules Parameters" *International Journal of Emerging Technology and Advanced Engineering*, 4(8), 311 - 318.
- Fraunhofer Institute for Solar Energy Systems, I (2017) *Photovoltaics Report*, Freiburg.
- Green, MA (1982) *Solar cells: operating principles, technology, and system applications*, Prentice-Hall.
- Gupta, MC & Ballato, J (2006) *The Handbook of Photonics, Second Edition*, CRC Press.

- Hejri, M, Mokhtari, H, Azizian, MR & Söder, L (2016), "An analytical-numerical approach for parameter determination of a five-parameter single-diode model of photovoltaic cells and modules" *International Journal of Sustainable Energy*, 35(4), 396-410.
- Hernandez, G (1988) *Fabry-Perot Interferometers*, Cambridge University Press.
- Humada, AM, Hojabri, M, Mekhilef, S & Hamada, HM (2016), "Solar cell parameters extraction based on single and double-diode models: A review" *Renewable and Sustainable Energy Reviews*, 56, 494-509.
- Imenes, AG & Mills, DR (2004), "Spectral beam splitting technology for increased conversion efficiency in solar concentrating systems: a review" *Solar Energy Materials and Solar Cells*, 84(1-4), 19-69.
- Iqbal, M 1983. Chapter 3 - The Solar Constant and its Spectral Distribution. *An Introduction to Solar Radiation*. Academic Press.
- Karp, J, Ford, JE, (Year)," Multiband Solar Concentrator using Transmissive Dichroic Beamsplitting ". paper presented at., 2008.
- Katsanevakis, M 2011. Modelling the photovoltaic module. *Industrial Electronics (ISIE), 2011 IEEE International Symposium on Industrial Electronics*. Gdansk, Poland: IEEE.
- Khalis, M, Masrour, R, Khrypunov, G, Kirichenko, M, Kudiy, D & Zazoui, M (2016), "Effects of Temperature and Concentration Mono and Polycrystalline Silicon Solar Cells: Extraction Parameters" *Journal of Physics: Conference Series*, 758, 012001.
- Khartchenko, NV & Kharchenko, VM (2013) *Advanced Energy Systems, Second Edition*, CRC Press.
- Klampaftis, E, Ross, D, McIntosh, KR & Richards, BS (2009), "Enhancing the performance of solar cells via luminescent down-shifting of the incident spectrum: A review" *Solar Energy Materials and Solar Cells*, 93(8), 1182-1194.
- Kost, C, Mayer, JN, Thomsen, J, Hartmann, N, Senkppiel, C, Philipps, S, Nold, S, Lude, S, Saad, N & Schlegl, T (2013) *Levelised Cost of Electricity - Renewable Energy Technologies*, Fraunhofer Institute for Solar Energy Systems ISE.
- Kreith, F, Krumdieck, S & Kreider, JF (2010) *Principles of Sustainable Energy*, CRC Press.
- MacLeod, HA & Macleod, HA (2010) *Thin-Film Optical Filters, Fourth Edition*, CRC Press.
- Mojiri, A, Taylor, R, Thomsen, E & Rosengarten, G (2013), "Spectral beam splitting for efficient conversion of solar energy—A review" *Renewable and Sustainable Energy Reviews*, 28, 654-663.
- National Energy Research Laboratory (NREL) (2017), "Best Research-Cell Efficiencies" <https://www.nrel.gov/pv/assets/images/efficiency-chart.png> [2017, May 9].
- Nelson, J (2003) *The Physics of Solar Cells*, Imperial College Press.

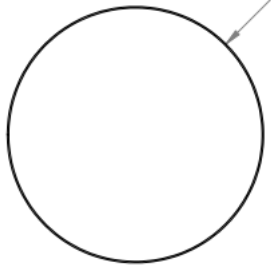
- Osborn, DE, Chendo, MAC, Hamdy, MA, Luttmann, F, Jacobson, MR, MacLeod, HA & Swenson, R (1986a), "Spectral selectivity applied to hybrid concentration systems" *Solar Energy Materials*, 14(3), 299-325.
- Osborn, DE, Chendo, MAC, Hamdy, MA, Luttmann, F, Jacobson, MR, MacLeod, HA & Swenson, R (1986b), "Spectral selectivity applied to hybrid concentration systems" *Solar Energy Materials*, 14(3-5), 299-325.
- Otanicar, TP, Phelan, PE, Prasher, RS, Rosengarten, G & Taylor, RA (2010), "Nanofluid-based direct absorption solar collector" *Journal of Renewable and Sustainable Energy*, 2(3), 033102.
- Otanicar, TP, Taylor, RA & Telang, C (2013), "Photovoltaic/thermal system performance utilizing thin film and nanoparticle dispersion based optical filters" *Journal of Renewable and Sustainable Energy*, 5(3), 033124.
- Overstraeten, R & Mertens, R (1986) *Physics, technology and use of photovoltaics*, Adam Hilger, Bristol.
- Pagliaro, M, Palmisano, G & Ciriminna, R (2008) *Flexible Solar Cells*, Wiley.
- Pérez-Higueras, P & Fernández, EF (2015) *High Concentrator Photovoltaics: Fundamentals, Engineering and Power Plants*, Springer International Publishing.
- Phang, J, Chander, D & Philips, S (1984), "Accurate analytical method for the extraction of solar cell model parameters" *Electronics letters*, 20(10), 406-408.
- Python (2015), "Scipy package" <https://www.python.org/downloads/release/python-351/> [2015].
- Rogalski, A, Adamiec, K & Rutkowski, J (2000) *Narrow-gap Semiconductor Photodiodes*, SPIE Press.
- Sara, ID, Betts, TR & Gottschalg, R (2014), "Determining spectral response of a photovoltaic device using polychromatic filters" *IET Renewable Power Generation*, 8(5), 467-473.
- Singh, P, Singh, SN, Lal, M & Husain, M (2008), "Temperature dependence of I-V characteristics and performance parameters of silicon solar cell" *Solar Energy Materials and Solar Cells*, 92(12), 1611-1616.
- Soulayman, S (2017) *Economical and Technical Considerations for Solar Tracking: Methodologies and Opportunities for Energy Management: Methodologies and Opportunities for Energy Management*, IGI Global.
- Stanley, C, Morjiri, A & Rosengarten, G (2016), "Spectral light management for solar energy conversion systems" *Nanophotonic*, 5(1), 169-179.
- Sze, S (1981) *Physics of Semiconductor Devices*, John Wiley & Sons, Murray Hill, New Jersey.

- Thelen, A (1970), "Design of Optical Minus Filters" *Journal of the Optical Society of America*, 61, 365.
- Thorlabs.com (2016), "Shortpass Dichroic Mirrors/Beamsplitters: 1000 nm Cutoff Wavelength" [https://www.thorlabs.com/newgrouppage9.cfm?objectgroup\\_id=9240](https://www.thorlabs.com/newgrouppage9.cfm?objectgroup_id=9240) [2016, 8th August].
- Vignola, F, Michalsky, J & Stoffel, T (2016) *Solar and Infrared Radiation Measurements*, CRC Press.
- Wysocki, JJ & Rappaport, P (1960), "Effect of Temperature on Photovoltaic Solar Energy Conversion" *Journal of Applied Physics*, 31(3), 571-578.

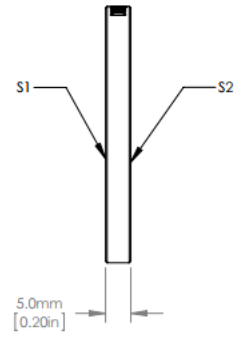


## 8. Appendix

### A. Optical filter (product specification)



$\phi 50.8\text{mm}$   
[2.00in]




S1 S2  
5.0mm  
[0.20in]

NOTES/SPECIFICATIONS:

1. CLEAR APERTURE:  $\geq 90\%$  OF DIAMETER
2. SURFACE QUALITY: 40-20 SCRATCH-DIG
3. TRANSMITTED WAVEFRONT DISTORTION:  
 $\lambda/4$  @ 633nm OVER CLEAR APERTURE
4. PARALLELISM:  $\leq 3$  arc min OVER CLEAR APERTURE
5. REFLECTION BAND (R):  
 $> 90\%$  ABSOLUTE 1020-1550nm
6. TRANSMISSION BAND (T):  
 $> 90\%$  AVERAGE,  $> 85\%$  ABSOLUTE 520-985nm
7. FILTER COATING (S1)
8. AR COATING (S2)
9. R:  $< 2\%$  ABSOLUTE 520-985nm  
AOI:  $45^\circ$

FOR INFORMATION ONLY  
NOT FOR MANUFACTURING PURPOSES

DRAWING PROJECTION					<b>THORLABS</b> www.thorlabs.com	
NAME	DATE	$\phi 50.8\text{mm}$ DICHROIC MIRROR, SHORT PASS 1000nm				
DRAWN TW	17/OCT/11					
APPROVAL DD	17/DEC/12	MATERIAL		REV		
COPYRIGHT © 2011 BY THORLABS		UV GRADE FUSED SILICA		D		
VALUES IN PARENTHESIS ARE CALCULATED AND MAY CONTAIN ROUND OFF ERRORS		ITEM #	APPROX WEIGHT			
		DMSPI000L	0.12 kg			

### B. Model Code

```

from math import exp
import numpy
import math
from scipy.optimize import fsolve
import scipy.optimize
import matplotlib.pyplot as plt
import pylab
import openpyxl
import os

#Intensity from height

def par_ext(Voc, Isc, Vmp, Imp, Ns, Ao_ref, G, T): #Parameter
Extraction

#PARAMETERS
q = 1.602e-19
k = 1.381e-23
T_ref = 299 #K
Eg = 1.12

```

```

Vt = k*T_ref/q

a_3 = Ao_ref * Ns
#Illumination Characteristics
G_ref = 980.0 #1013.28680869 #W/m^2
mu_sc = 0.0
Iph_ref = Isc #A

def f(variables):
    (Rs,Rsh) = variables
    y = -Imp*(1+(Rs/Rsh)) + ((-Voc + (Rs +
Rsh)*Isc)/Rsh)*(1 - numpy.exp((Vmp - Voc +
Rs*Imp)/(a_3*Vt)))+(Voc - Vmp)/Rsh
    z = (-Rs/Rsh) + (Rsh - Rs)/(a_3 * Vt) * ((-Voc + (Rs +
Rsh)* Isc)/Rsh)*numpy.exp((Rs*Isc - Voc)/(a_3*Vt))
    return [y,z]

D_1 = fsolve(f,[abs(0.5),abs(400)])
Rs = D_1[0]
Rsh = D_1[1]*(G_ref/G)
Ao = Ao_ref *(T/T_ref)
Vt = k*T/q
#Calculating Iph
#Iph
Iph = (G/G_ref)*(Iph_ref + mu_sc *(T - T_ref))
print('Iph = (2015) '.format(Iph))

#Calculating Io"""
Io_ref = Isc * numpy.exp(-Voc/(Ns*Vt*Ao))
Io = Io_Hab*exp((q*Eg/(Ao*T))*(1/T_ref) -
(1/T)))*(T/T_ref)**3

nNsVt = Ao * Ns * Vt

print('Rs = {}'.format(Rs))
print('Rsh = {}'.format((Rsh)))
print('Ao = {}'.format((Ao)))
print('nNsVt = {}'.format((nNsVt)))
print "Io =", (Io)
parameters = Iph,Io,Rs,Rsh,nNsVt

return parameters

#import excel data

```

```

import_data = openpyxl.load_workbook('C:\Users\user\Google
Drive\Masters\CPV\Experimental data\Churchill\Filter at
50cm\Model data for python.xlsx')
print import_data

import_data.get_sheet_names()
A_1 = import_data.get_sheet_by_name('Sheet2')

source = [A_1]
import_data.active

voltage = []
current = []

for i in range(len(source)):
    Column_length = len(source[i]['A'])
    print Column_length
    for j in range(Column_length):
        voltage = voltage +
[source[i].cell(row=j+1,column=1).value]
        current = current +
[source[i].cell(row=j+1,column=2).value]

G = 960.0
print "light intensity", G
Ao_ref = 1.3
#Extract Parameters
l = F_C = par_ext(0.61,0.188,0.429411,0.168363,1,Ao_ref,G,299)

#Plot IV CURVE
iv_data_l =
pvlib.pvsystem.singlediode(l[0],l[1],l[2],l[3],l[4],ivcurve_pn
ts = 50)
cell_area = (0.053 * 0.018) #M^2
max_power = iv_data_l['i_mp'] * iv_data_l['v_mp']
P_in = G * cell_area
Eff = max_power/P_in
FF = max_power/(iv_data_l['i_sc'] * iv_data_l['v_oc'])
print "Isc_new",iv_data_l['i_sc']
print "Max Power", max_power
print "Efficiency", Eff
print "Fill Factor", FF

#print iv_data
#print (voltage,current)
plt.plot(voltage,current, ".")
#plt.plot(iv_data_b['v'], iv_data_b['i'])
plt.plot(iv_data_l['v'], iv_data_l['i'])
for i in range(50):

```

```
print iv_data_1['v'][i], iv_data_1['i'][i]  
plt.show()
```

r